To the Graduate Council:

I am submitting herewith a thesis written by Joseph L. Orr entitled "SSME Nozzle Flow Field Calculations Using PARC CFD Code." I have examined the final copy of this thesis for form and content and recommend that it be accepted in partial fulfillment of the requirements for the degree of Master of Science, with a major in Mechanical Engineering.

Frank G. Collins
Major Professor

We have read this thesis
and recommend its acceptance:

A.D. Vakili

Gw Garrison

Accepted for the Council:

Vice Provost
and Dean of The Graduate School

STATEMENT OF PERMISSION TO USE

In presenting this thesis in partial fulfillment of the requirements for a Master's degree at the University of Tennessee, Knoxville, I agree that the Library shall make it available to borrowers under rules of the Library. Brief quotations from this thesis are allowable without special permission, provided that accurate acknowledgement of the source is made.

Permission for extensive quotation from or reproduction of this thesis may be granted by my major professor, or in his absence, by Head of Interlibrary Services when, in the opinion of either, the proposed use of the material is for scholarly purposes. Any copying or use of the material in this thesis for financial gain shall not be allowed without my written permission.

Signature Joseph L. Orr

Date August 19, 1989

SSME NOZZLE FLOW FIELD CALCULATIONS USING PARC CFD CODE

A Thesis

Presented for the

Master of Science

Degree

The University of Tennessee, Knoxville

Joseph L. Orr

December,1989

AKNOWLEDGEMENTS

The author would like to thank the following people for contributing to the development of this research and thesis. Without their help the end result would not have been possible.

Dr. Frank Collins. Dr. Collins provided more than the general assistance needed to perform the research. He introduced the author to a network of experienced persons whose advice was enormously helpful to the research effort. His experience with gas dynamics helped to solve many of the problems which surfaced during the research.

Kyle Cooper. Kyle answered all the tough questions concerning the PARC code. His advice eliminated many of the problems encountered by a first-time computational fluid dynamics code user.

Peter Liver. With Mr. Liver's permission his artificial dissipation model was used as part of this research. As a PARC and INGRID computer code user, he was able to provide insight into the problems encountered when running the codes.

The employees of CASP. The people at CASP provided daily support in terms of computer hardware, word processing, research funding, and most important, cooperation.

ABSTRACT

The purpose of this research is to validate the use of the PARC computational fluid dynamics (CFD) computer code to calculate the rocket nozzle flow fields and relative performance levels for the Space Shuttle Main Engine (SSME).

Three SSME nozzle flow fields (inviscid, laminar, and turbulent) were calculated using the PARC code. The results were compared to existing data and/or theoretical calculations in order to validate the code.

This thesis describes the process of generating a flow field solution with the PARC code. The generation of the computational grid, the choice of the PARC code inputs, and the user's interaction with the PARC code required to achieve a converged flow field solution are discussed.

The results of the research show that the PARC code inviscid flow field calculations compare well with existing data generated by a highly regarded computational fluid dynamics code. The viscous PARC results show good correlation with theoretical and empirical calculations. The capability of the PARC code as a rocket nozzle design tool was demonstrated by calculating and contrasting the nozzle performance parameters for the various nozzle flow field solutions.

TABLE OF CONTENTS

CHAPTER		PAGE
I.	INTRODUCTION	1
II.	COMPUTATION CODES	6
	PARC Code	6
	INGRID Code	8
	Plotting Program	9
	Computer System	10
III.	INVISCID CALCULATIONS	11
IV.	LAMINAR CALCULATIONS	23
V.	TURBULENT CALCULATIONS	46
VI.	CONCLUSIONS	59
BIBLIOGRAPHY		63
APPENDIXES		66
	A. COMPUTATION PROCEDURES	66
	B. NOZZLE PERFORMANCE SUBROUTINE EQUATIONS	87
	C. SAMPLE CALCULATIONS	92
VITA		98

LIST OF FIGURES

FIGURE		PAGE
1.	Computational Grid for Case 1.....	12
2.	Mach Number Contours for Case 1.....	15
3.	Sonic Line for Case 1 Inviscid Flow Calculations.....	18
4.	Comparison of Mach Number Distributions	20
5.	Computational Grid for Case 2.....	26
6.	Shock-Capturing Grid Comparison.....	27
7.	Effect of Artificial Dissipation on Solution.....	31
8.	Laminar Boundary Layer Velocity Profiles	36
9.	Laminar Boundary Layer Temperature Profiles.....	40
10.	Law of the Wall Parameters.....	50
11.	Boundary Layer Temperature Profile Comparison.....	54
12.	Boundary Layer Velocity Profile Comparison.....	55

FIGURE PAGE

A-1. Generic Sketch of Grid Boundaries and Patches..... 67

A-2. Sample PARC Re-start File..... 72

A-3. Sample of PARC Interactive Output File.. 78

A-4. Sample of PARC Interactive Output File Flow Properties..... 84

B-1. Computer Code of Performance Subroutine 90

LIST OF TABLES

TABLE		PAGE
III-1	Inviscid Performance Parameters . . .	20
IV-1	Laminar Performance Parameters . . .	43
A-1	Exit Plane Turbulent Boundary Layer Percent Changes	85

CHAPTER I

INTRODUCTION

The purpose of this research was to validate the use of the PARC computational fluid dynamics (CFD) code to generate accurate flow fields and relative performance levels for the Space Shuttle Main Engine (SSME) rocket nozzle. Inviscid, laminar, and turbulent nozzle flow fields were generated using the PARC code and the results were compared to existing data or theoretical calculations.

This research is the first part of a multi-phase effort between the Center for Advanced Space Propulsion (CASP) and Rocketdyne to enhance the PARC code for use as a high-area-ratio nozzle design tool. Before the PARC code is enhanced by adding, among other items, non-equilibrium chemistry and exit rarefaction, the nozzle flow field calculations generated by the PARC code must be validated. The SSME nozzle was chosen as a validation test case.

The standardized Joint Army, Navy, NASA, and Air Force (JANNAF) methodology [1][1] for calculating rocket

---

[1] Numbers in brackets refer to similary numbered references in the Bibliography.

nozzle flow fields and performance has two comparable procedures. One procedure is a series of disjoint computer codes which contribute specialized information to the over-all nozzle flow field calculation. One-Dimensional Equilibrium Program (ODE), One-Dimensional Kinetics Program (ODK), and Boundary Layer Integral Matrix Procedure Program (BLIMP) are some of the codes which constitute the disjoint procedure. The other procedure integrates contributing codes into one large code called; Two-Dimensional Kinetics Program (TDK) [2]. Subprograms within TDK provide essentially the same information as the disjoint codes in the initially discussed procedure, yet in a more cohesive manner.

Investigation of the validity of the JANNAF methodology to high-area-ratio rocket nozzle calculations has been conducted by various organizations. Individual studies have resulted in modifications to the JANNAF procedure to improve its modelling of the high-area-ratio nozzle flow environments [3]. Results of tests comparing JANNAF methodology calculations to experimental data show that the JANNAF method does a good job of predicting over-all nozzle performance for nozzle area ratios up to 1000 [4]. However, detailed analysis of viscous effects within the JANNAF calculations show that there is room for improvement in the area of viscous modelling and heat transfer [5,6]. Also, generating solutions with the JANNAF codes

is an involved, time-consuming process. Generally, the JANNAF methods lack the flexibility and efficiency needed for a nozzle design code.

The justification for this research is that current Joint Army, Navy, NASA, and Air Force (JANNAF) rocket nozzle computational methodology is inadequate for nozzles with thick boundary layers. JANNAF methodology assumes the nozzle boundary layers are thin and can be computed separately (uncoupled from the core flow calculations). As the nozzle area increases and the boundary layers within them become thicker, uncoupling the boundary layer and core flow calculations result in viscous/inviscid interaction errors, or viscous drag errors. This creates uncertainty in predicted nozzle performance.

The PARC code is a general purpose full Navier-Stokes equation solver developed at Arnold Engineering Development Center (AEDC). The importance of solving the Navier-Stokes equations for this application was that the core and boundary layer regions can be solved simultaneously, not in an uncoupled fashion as in the JANNAF methodology mentioned above. Also, Navier-Stokes equation solutions have exhibited the best correlation to experimental flow field data, especially when the flows have complex shock structures like high-area-ratio nozzles.

The trend for future rocket nozzles is towards larger area ratios. The advantages of high-area-ratio nozzles

are increased high-altitude (space) performance and larger payloads. The PARC code could be used as a tool during the design of future nozzles. The PARC code could minimize the amount of experimental testing of prototype nozzle designs for performance trends and decrease the uncertainty of predicted nozzle performance. The PARC code is also widely used in the propulsion field and its popularity is increasing [7,19].

The boundary layers of the SSME nozzle were not thick enough to create adverse interactions with the nozzle core flow. Nonetheless, the SSME nozzle was a good test case to validate the PARC code viscous flow calculations.

Three SSME nozzle flow fields were calculated using the PARC code: inviscid, laminar and turbulent. The inviscid PARC flow field solution was compared to computations performed by Rocketdyne. The laminar and turbulent flow field calculations were compared to theoretical and empirical calculations. Only two-dimensional PARC computations were performed on the SSME nozzle during this research due to the nozzle's axisymmetry. The following assumptions made for all PARC nozzle flow field calculations were:

1. nozzle fluid is a perfect gas;
2. constant ratio of specific heats and Prandtl number;
3. non-reacting nozzle fluid;

4. adiabatic nozzle wall;
5. steady nozzle flow;
6. internal nozzle flow only, no external flow or interactions.

The PARC code was modified during this study to calculate mass flow, thrust, and specific impulse for nozzle performance level evaluation. Absolute performance levels could not be calculated because real gas effects and thermodynamics are presently not treated within the PARC code. However, the relative performance levels were useful in validating the PARC flow field calculations.

The INGRID computer code was used to generate the computational grid for the PARC code. Like the PARC code, INGRID was developed and obtained from AEDC.

An integral part of the research effort was learning how to utilize the PARC and INGRID codes. The procedures used to run the codes as well as some insight on how they can be run effectively are described.

CHAPTER II

COMPUTATION CODES

PARC Code

The PARC code is a modified version of the ARC code developed at the NASA Ames Research Center [8]. The PARC code used in this research was obtained from AEDC. A thorough description of the PARC code is included in [9]. The following paragraphs briefly describe major features of the code.

The PARC code is a finite difference flow field simulation computer program. The system of differential equations for the code are the Reynolds-averaged Navier-Stokes equations expressed in nondimensional conservative form. The code assumes that the fluid: is a perfect gas, obeys Sutherland's viscosity law, and has a constant Prandtl number.

One of the features of the PARC code is the Beam and Warming implicit approximate factorization scheme. Artificial viscosity exists in this scheme to ensure numerical stability and to dampen high frequency oscillations in the flow field solution. The significance of artificial dissipation will be discussed in the Laminar Calculations chapter.

The PARC code allows various fluid viscosity options. Inviscid, laminar, and turbulent flow fields can be calculated with the code. One can designate viscosity in the axial direction, in the radial direction, or in both directions. Of course, fluid viscosity can be removed altogether for inviscid flow field calculations.

All flow field calculations were done with the PARC code containing the latest algebraic Baldwin/Lomax turbulence model and artificial dissipation upgrades.

The output from the PARC code is contained in two files. One file, called the interactive output file (IOF), contains the calculated values of temperature, pressure, Mach number, and other flow properties, at all grid points within the flow field. The values of the flow properties are in engineering units. The other file, called the re-start file, contains non-dimensionalized flow properties at all grid points. This file is used as the PARC code input file for the next group of iterations.

Appendix A describes the inputs and convergence process to generate the nozzle flow field solution with the PARC code.

The PARC code was upgraded during this research by adding a subroutine to calculate the following nozzle performance parameters: mass flow, thrust, and specific impulse. The purpose of the performance subroutine was to

improve the PARC code as a nozzle design tool. The interest was in observing the difference in nozzle performance with boundary layer viscous effects. This subroutine was also used to help determine the validity of the PARC flow field computations. The performance subroutine integrates the flow properties along a designated plane in the nozzle (usually the exit plane) using Simpson's Composite Algorithm. Formulation of the performance subroutine is included in Appendix B.

INGRID Code

The INGRID code used in this research was obtained from AEDC. A detailed description of the code is included in [10]. A short description of the INGRID code follows.

INGRID is an interactive, two-dimensional, algebraic grid generation code. The code has many options to generate grids for various geometries and also contains many grid clustering and smoothing options. Interpolation techniques within INGRID minimize the number of inputs required to define a given geometry/grid situation.

A distinct feature of the INGRID program is the concept of a history file. The interactive inputs to the INGRID program are saved in an input history file. The grid can be recreated by transferring the history file to the INGRID program. This eliminates the process of rerun-

ning the INGRID program when minor errors or changes have been made. The history file simplifies the grid modification or optimization process and saves memory space when working with many different grids.

Another attractive feature of the INGRID program is its compatibility with the PARC code. The output from INGRID can easily be formatted for input to the PARC code.

Appendix A summarizes the procedure of generating a computational grid with the INGRID code.

Plotting Program

PLOT3D was the plotting program used to generate the flow field parameter contour plots. This program was written by Pieter Buning at NASA Ames Research Center. PLOT3D is compatible with the PARC code. The formats for the data input and output are the same for the two codes. Unfortunately, the PLOT3D program assumes that gamma is 1.4. Thus, although the contour plots show all the distinguishing features of the flow fields, the magnitudes of the contour lines are not correct due to PLOT3D's gamma assumption.

Computer System

All the calculations with the PARC code were performed on the CRAY X-MP416 system at NASA Marshall Space Flight Center. An IBM 3084 was the front-end computer for the CRAY and was accessed from a VISUAL 603 terminal at the University of Tennessee Space Institute (UTSI) via a telephone modem. The VISUAL terminal was chosen for its VT100 emulation and TEKTRONIX graphics capabilities. Hard-copy of the PARC solutions was self-couriered from NASA Marshall on a weekly basis.

CHAPTER III

INVISCID CALCULATIONS

The objective of the inviscid SSME nozzle computations was to compare the solutions for the PARC code to those computed by Rocketdyne. The Rocketdyne solution was generated using its Euler code developed at the Rockwell Science Center. The Rocketdyne data has been compared to data generated by the current Joint Army-Navy-NASA-Air Force (JANNAF) methodology for calculating rocket nozzle flow fields and showed good agreement. The JANNAF methodology is a 'yardstick' upon which many nozzle CFD codes are compared. Thus the Rocketdyne data provides a 'link' to the accepted methodology of calculating inviscid rocket nozzle flow fields. A good correlation between the PARC solution and the Rocketdyne data therefore was a means of validating the PARC calculations.

The first computational grid, called Case 1, for the inviscid calculations had 203 grid points in the axial direction (from injector plane to nozzle exit plane) and 100 points in the radial direction (centerline of nozzle wall). Grid points were packed within the nozzle throat region and along the nozzle centerline. This grid will be referred to as Case 1. See Figure 1 for plots of sections of the Case 1 grid.

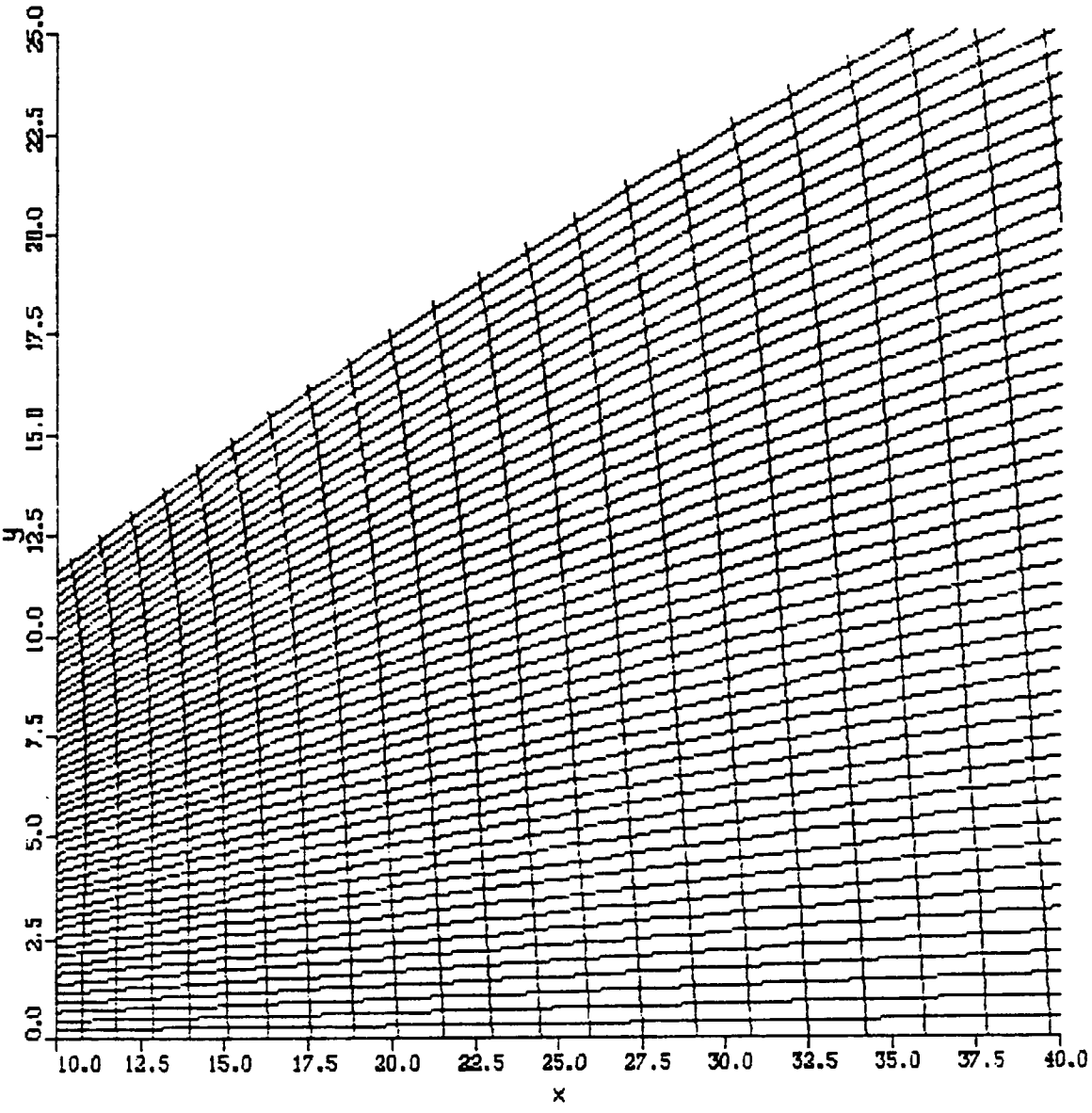


Figure 1. Computational Grid for Case 1.

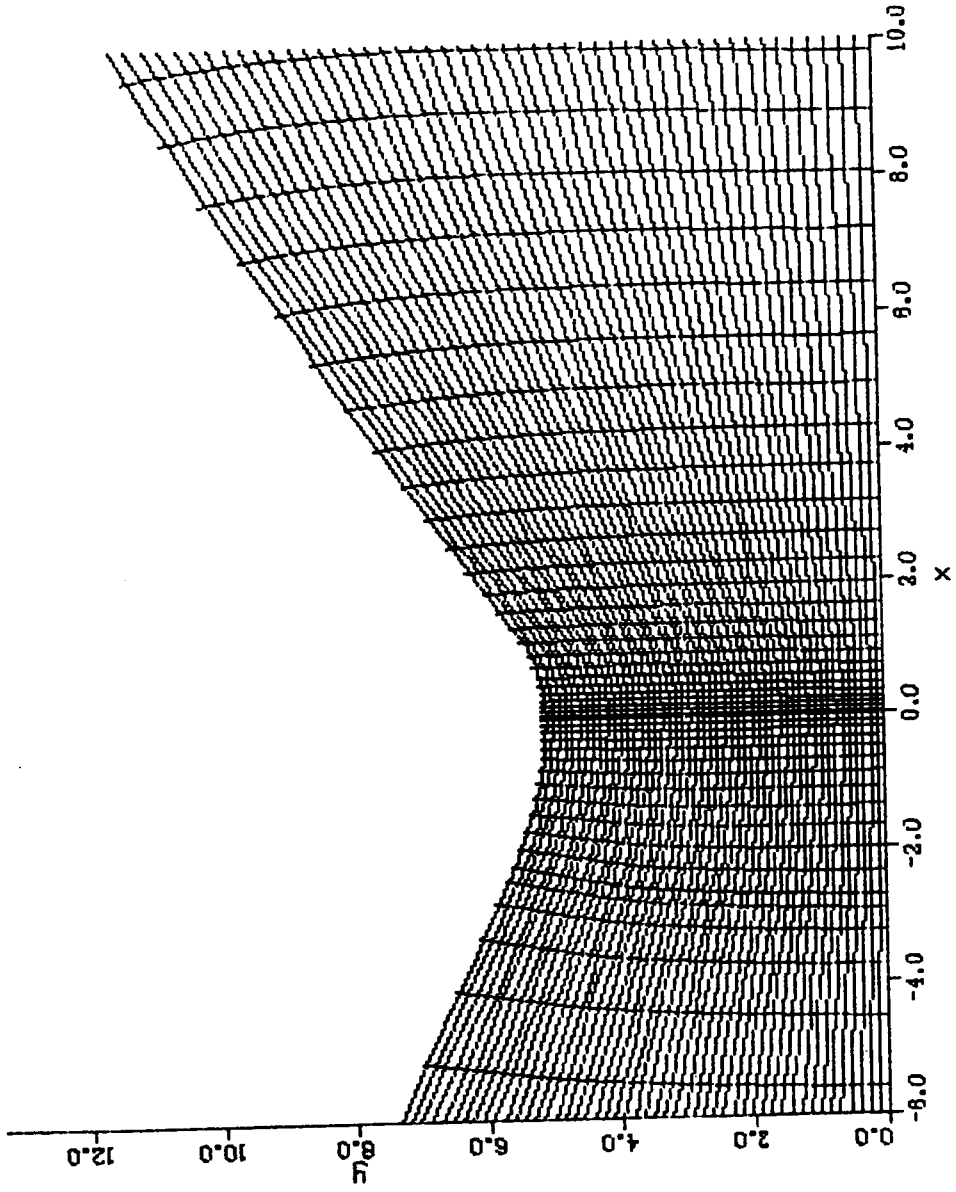


Figure 1. (Continued) Throat Region

Rocketdyne supplied the SSME nozzle operating conditions as:

Total Pressure= 3000 psia,

Total Temperature= 6600 R,

Specific Heat Ratio= 1.2,

Exit Pressure= 0.03 psia.

Other fluid properties for the inviscid, laminar, and turbulent calculations are listed in Appendix A.

The convergence process was monitored by observing the convergence statistics (defined in Appendix A) of the PARC code output every tenth iteration. The time step (DTCAP) was the only PARC input parameter which was altered during the convergence process. Viewing the PARC flow field output revealed that the nozzle flow field was well established after 4000 iterations. At this point DTCAP was lowered from its original value of 5 to the end value of 2 over a 2000 iteration interval. The converged inviscid flow field solution was achieved within 6000 iterations. The truncation error level (L2) for the converged solution was 10E-10. A description of the convergence process is included in Appendix A.

Mach number contours generated by PLOT3D for the converged PARC inviscid flow field solution on the Case 1 grid are shown in Figure 2. Interesting characteristics of the Mach number contours are the apparent smearing of

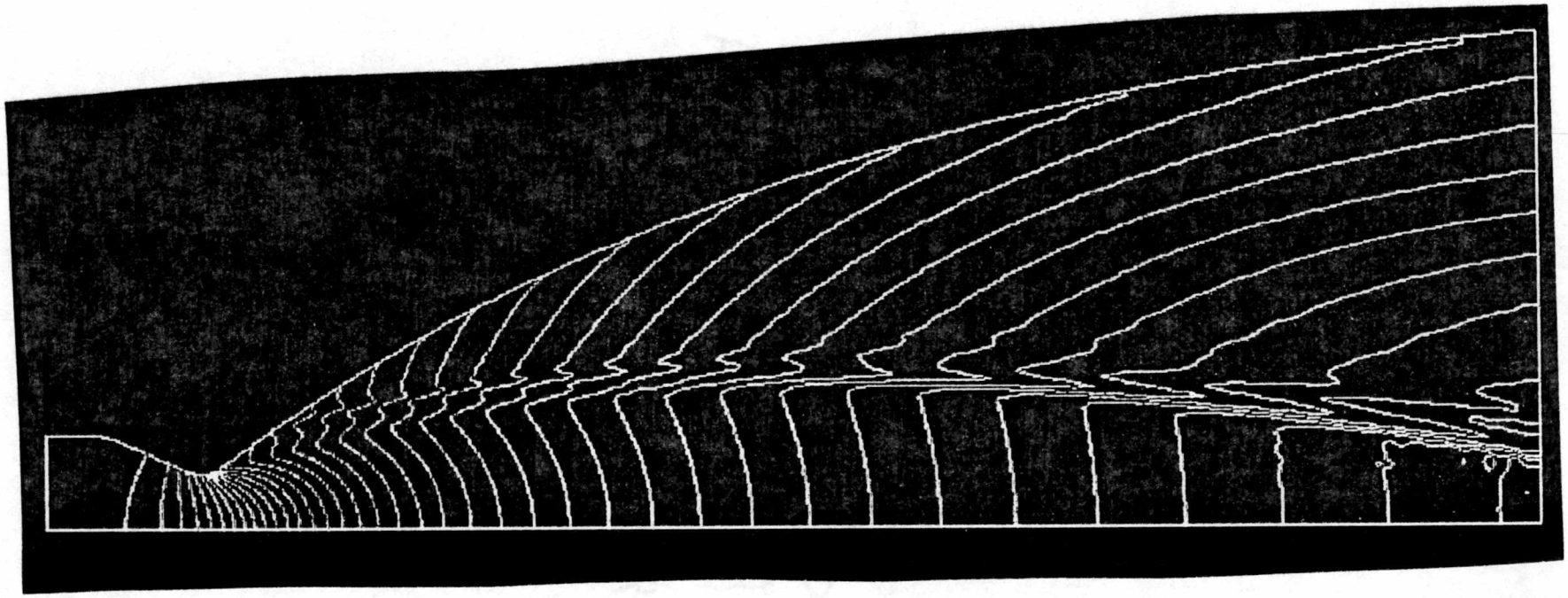


Figure 2. Mach Number Contours for Case 1.

the shock over several grid mesh intervals and the oscillations which occur near the shock. These are inherent characteristics of the Beam and Warming shock capturing numeric algorithms within the PARC code. Although these characteristics exist, the Beam and Warming algorithms are known to give the correct shock locations [11]. The amount of smearing and oscillations could be minimized by interactively varying the amount of damping (artificial dissipation) in the shock-capturing algorithm within the PARC code during the solution convergence process. An experiment was done during the laminar calculations to improve the shock definition by packing the grid points in the shock region. This grid was called Case 2. See the Laminar Calculations chapter.

The transonic region within the throat of the SSME nozzle is a critical computation area. Figure 2 shows that the shock originates in the nozzle just down-stream from the nozzle throat. The origin of the shock is a discontinuity in the nozzle contour between the radius of curvature of the throat section and the parabolic shape of the expansion section. An error in the flow field calculation within the transonic region could conceivably affect the origin of the shock. Misplacement of the shock in the transonic region will affect the entire flow field calculation, and thus the nozzle's overall performance.

The integrity of the PARC solution in the transonic region was evaluated by looking at the sonic line calculation. The mathematics of the flow in the transonic region reveals interesting characteristics for the sonic line [12,14]. Because the nozzle throat wall radius of curvature was not constant for the SSME (it changes three times within the throat region), small perturbation series-expansion solutions of the potential flow equations were not easily applicable. Yet, the distinguishing features of the sonic line calculation were observed. A qualitative analysis of the sonic line calculation shows the following features:

1. The sonic line meets the nozzle wall upstream of the geometric throat.
2. The angle the sonic line makes with the nozzle wall is of the correct magnitude.
3. The sonic line is concave in the direction of the fluid flow.
4. The sonic line is perpendicular to the centerline (axis of symmetry).

All of the above were expected characteristics. Figure 3 is a plot of the sonic line calculated in the PARC solution.

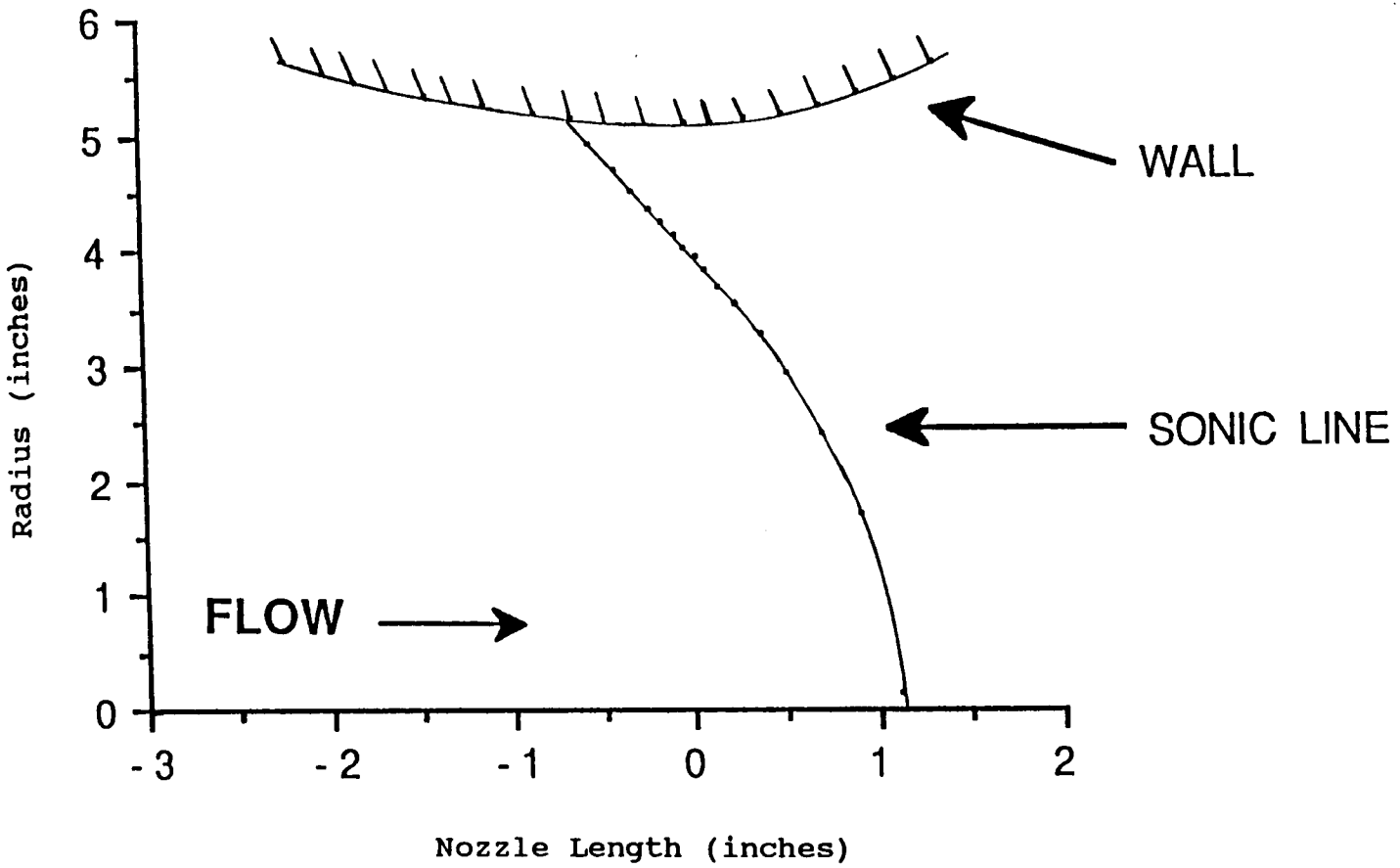


Figure 3. Sonic Line For Case 1 Inviscid Flow Calculations.

Comparison of the PARC and Rocketdyne Mach number distributions are in Figure 4 and show no discernible difference in Mach numbers along the wall. There were random, slight, differences along the centerline. Near the exit plane, where the maximum deviation occurred, the difference was within .4%. This small difference is interesting since both computation methods used different computational algorithms to generate the flow fields. The excellent agreement in calculated Mach number indicates that the PARC code provides acceptable inviscid flow field predictions for the SSME nozzle.

The PARC code inviscid flow field solution was also reviewed from a performance standpoint. Nozzle performance parameters such as mass flow, thrust, and specific impulse were determined from the PARC solution by integrating across the exit plane of the nozzle and were compared to ideal values. See APPENDIX B for a description of the integration process.

Ideal values for mass flow and specific impulse were calculated from one-dimensional, isentropic, perfect gas relations. Sample calculations are included in Appendix C.

The results of the inviscid performance calculations are presented in Table III-1. Note that there are two inviscid solutions. The Case 2 solution used an improved

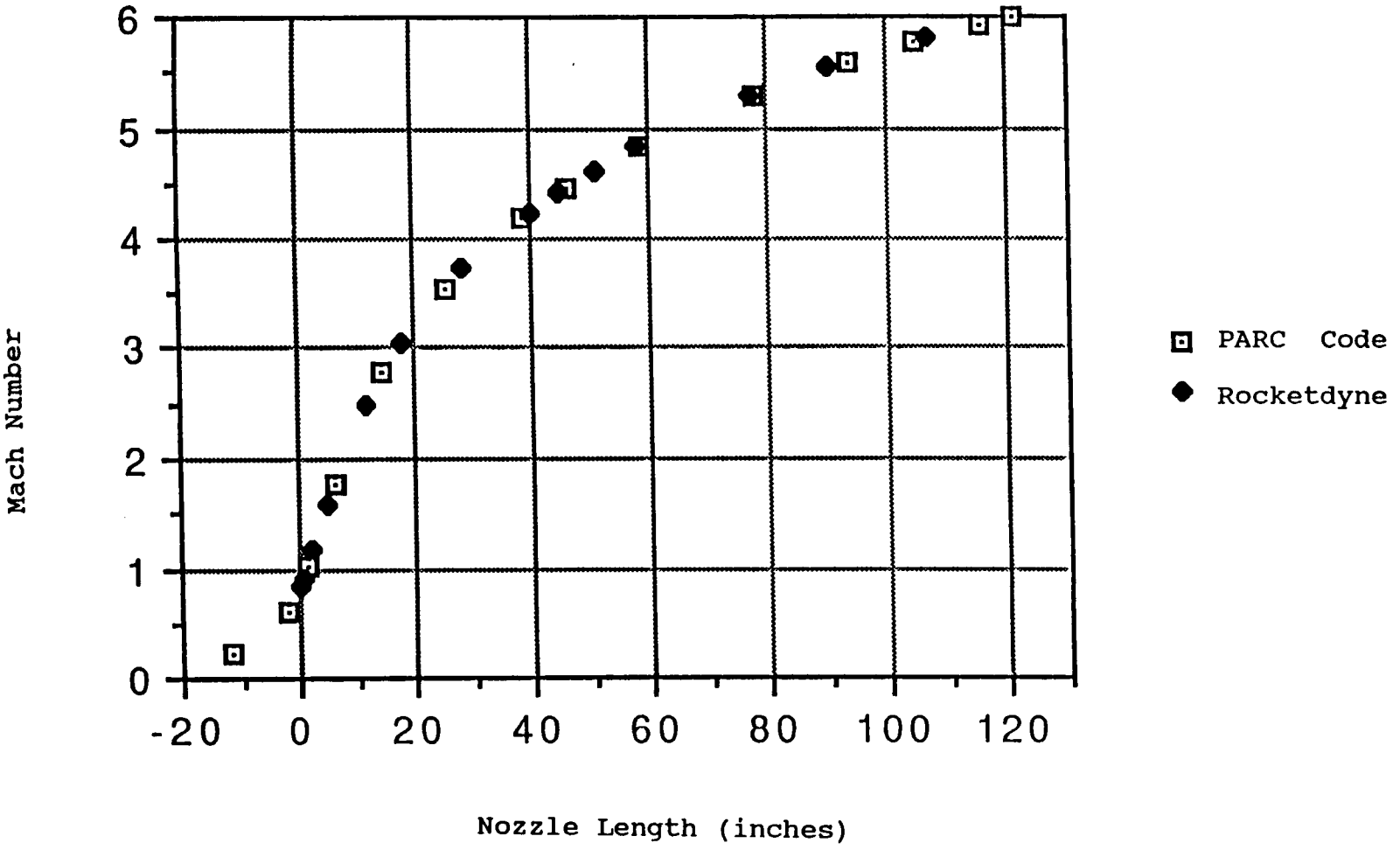


Figure 4. Comparison of Mach Number Distributions (Nozzle Wall).

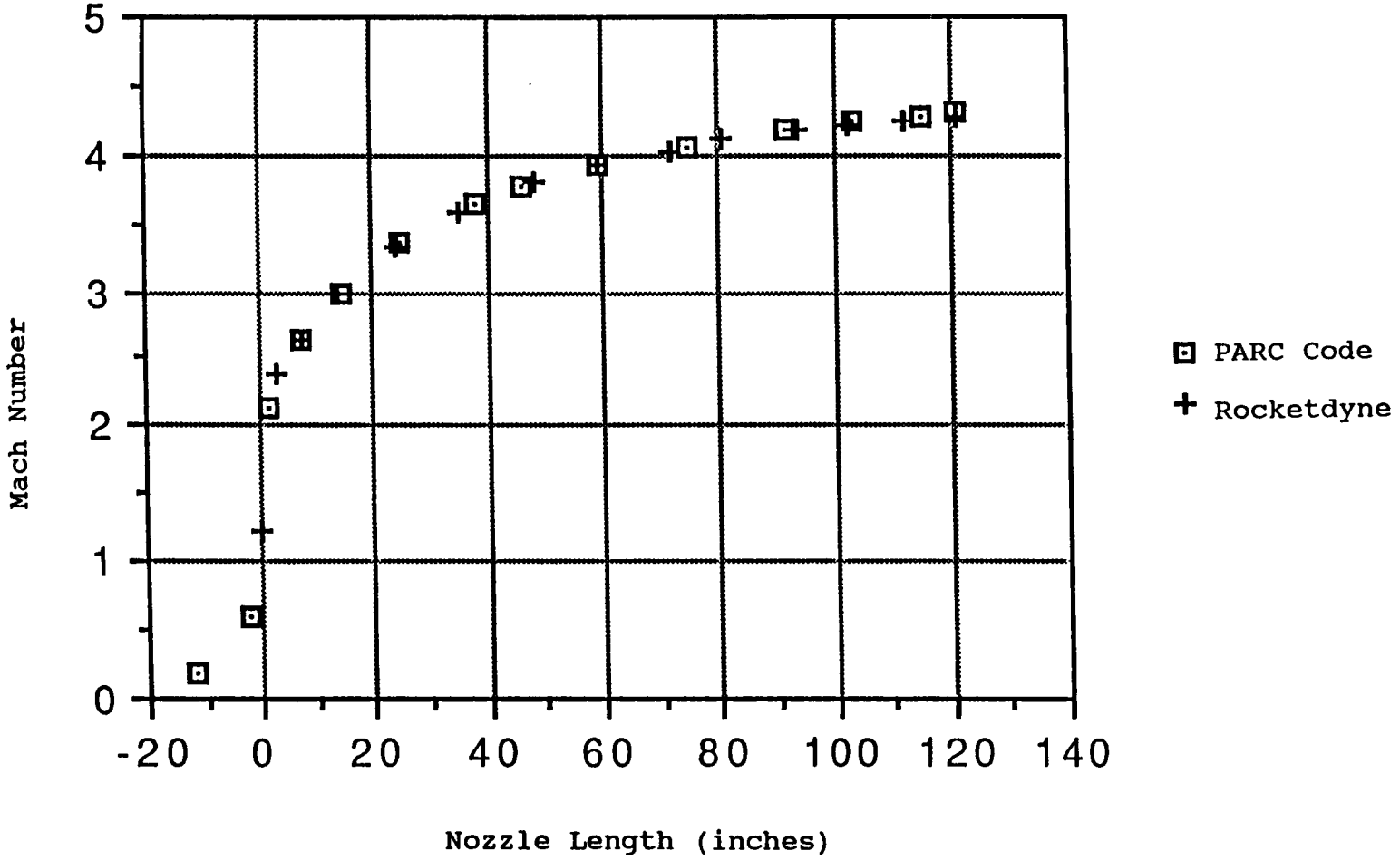


Figure 4. (Continued) (Nozzle Centerline)

grid with grid packing along the shock. Details of this grid are included in the Laminar Calculations chapter. The Case 2 grid improves upon the mass flow and thrust calculations of the original inviscid grid (Case 1) relative to the ideal values, thus showing the dependence of the solution upon the computational grid. The Case 2 flow field solution and performance levels were used for comparison to the laminar and turbulent results. The discrepency in thrust and specific impulse values between the PARC solutions and the ideal solution was due to the presence of the embedded shock within the nozzle and divergence loss at the nozzle exit.

Table III-1. Inviscid Performance Parameters

	m (lb/s)	F (x10E+5 lb_f)	Isp (sec)
Ideal	1223.5	5.077	424.4
Case 1	1186.0	4.661	393.0
Case 2	1210.0	4.763	392.7

CHAPTER IV

LAMINAR CALCULATIONS

The objective of the laminar calculations was to compare PARC flow field solutions to the PARC inviscid solution and to theoretical calculations. Validation of the PARC laminar solution was dependent on how well the data compared to the theoretical calculations and the inviscid PARC solution.

The laminar flow field calculations could be termed the 'experimental phase' of the code validation process. Establishing a convergence routine for the laminar solutions involved many trial and error attempts and in general was more difficult than the inviscid calculations to converge. Three different computational grids and an enhanced artificial dissipation model were experimented with to view their effect on the flow field calculations. The information gained from these experiments was applied to both the inviscid and turbulent flow field calculations to improve those flow field calculations.

An experiment with the computational grid was conducted during the laminar calculations to improve the resolution of the shock location within the nozzle. This grid will be referred as the Case 2 grid to distinguish it from other grids that will be discussed. The shock in

the inviscid solution (Case 1 grid) had the undesirable characteristic of being smeared over several grid points (See Figure 2, page 14). The smearing of the shock was undoubtedly biasing the inviscid nozzle performance calculations because the proportion of the nozzle area affected by the shock at the exit plane was too large.

The resolution of the shock could be improved by repacking the grid points in the vicinity of the shock. Ideally, one would like to eliminate the shock smearing and confine the influence of the shock to a very thin area along the length of the shock. After all, the thickness of a real shock wave is on the order of .0001 inch. To achieve this order of shock resolution would require more grid points and tighter packing along the shock. Fifteen grid points were packed along the length of the shock for the Case 2 grid. Grid packing along the shock was not pursued beyond the Case 2 grid due to the increased computation time and storage capacity required.

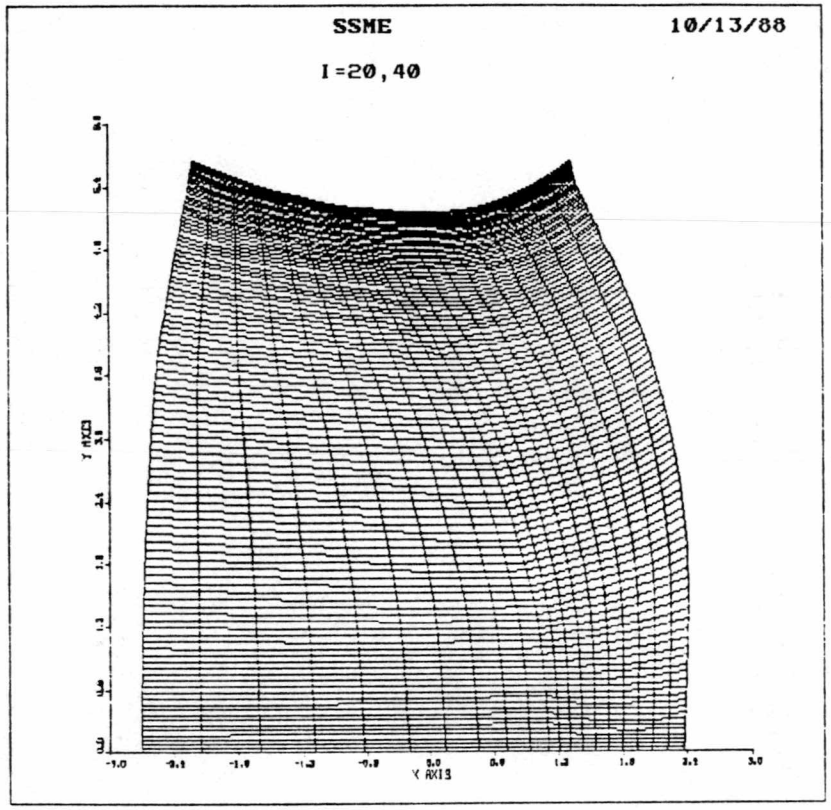
Another important feature of the Case 2 grid was the amount of grid packing towards the wall required to resolve the flow's boundary layer. Fifteen grid points within the laminar boundary layer was the minimum number chosen based on the experience of other PARC users [13]. Calculations were performed prior to the generation of the Case 2 grid to get an estimate of the boundary layer

thickness based on a flat plate analysis. This information was used to determine the packing needed to ensure at least fifteen points within the boundary layer. Figure 5 with Figure 1 on pages 11 and 12 show the contrast between the Case 2 grid and the Case 1 grid.

The final feature of the Case 2 grid was the forming of the grid lines within the transonic region of the nozzle to resemble the somic line. The purpose of this shape was to improve the PARC code calculations within this crucial flow region. It was believed that contouring the grid lines to resemble the actual flow characteristics would improve the PARC code's flow field solution.

The results of the grid experiment were that packing the grid in the shock region improves the resolution or sharpness of the shock. This is evident by contrasting the shocks in Figure 6. Tighter packing along the shock and more grid points in the axial direction should further improve the shock resolution. Forming the grid lines in the nozzle throat region to resemble the sonic line did not change the flow field calculations in that region. The sonic line was in the same location as the Case 1 grid.

The results of the Case 2 experiment were used to improve the inviscid flow field calculations (See the Inviscid Calculations chapter). An inviscid flow field solution was generated with the Case 2 grid. The performance parameters calculated on the Case 2 grid correlate



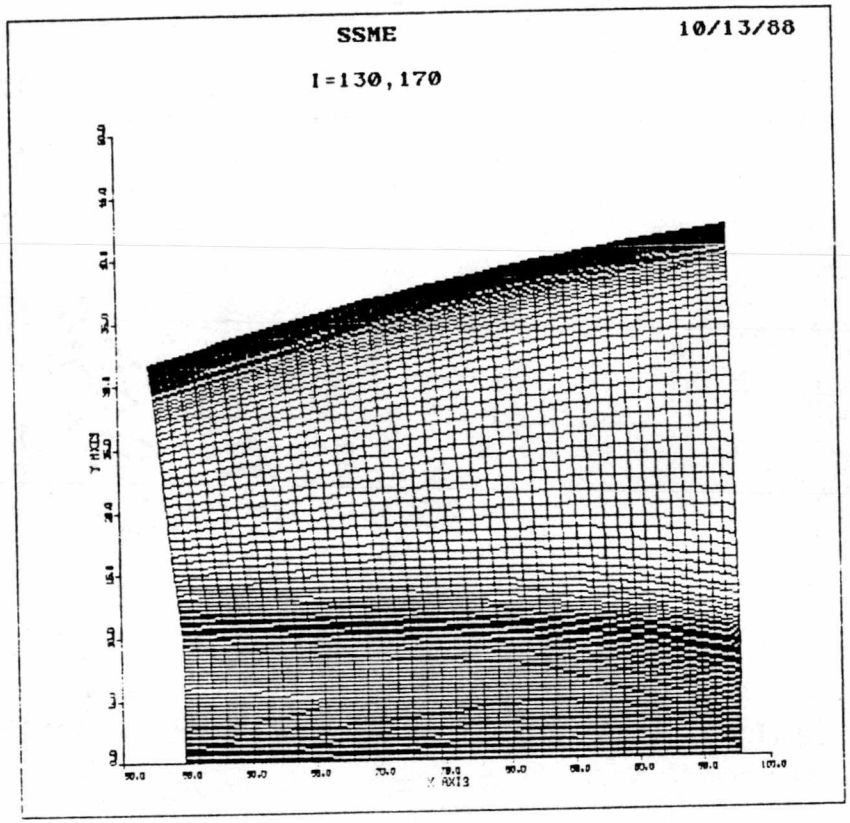


Figure 5. Computational Grid for Case 2.

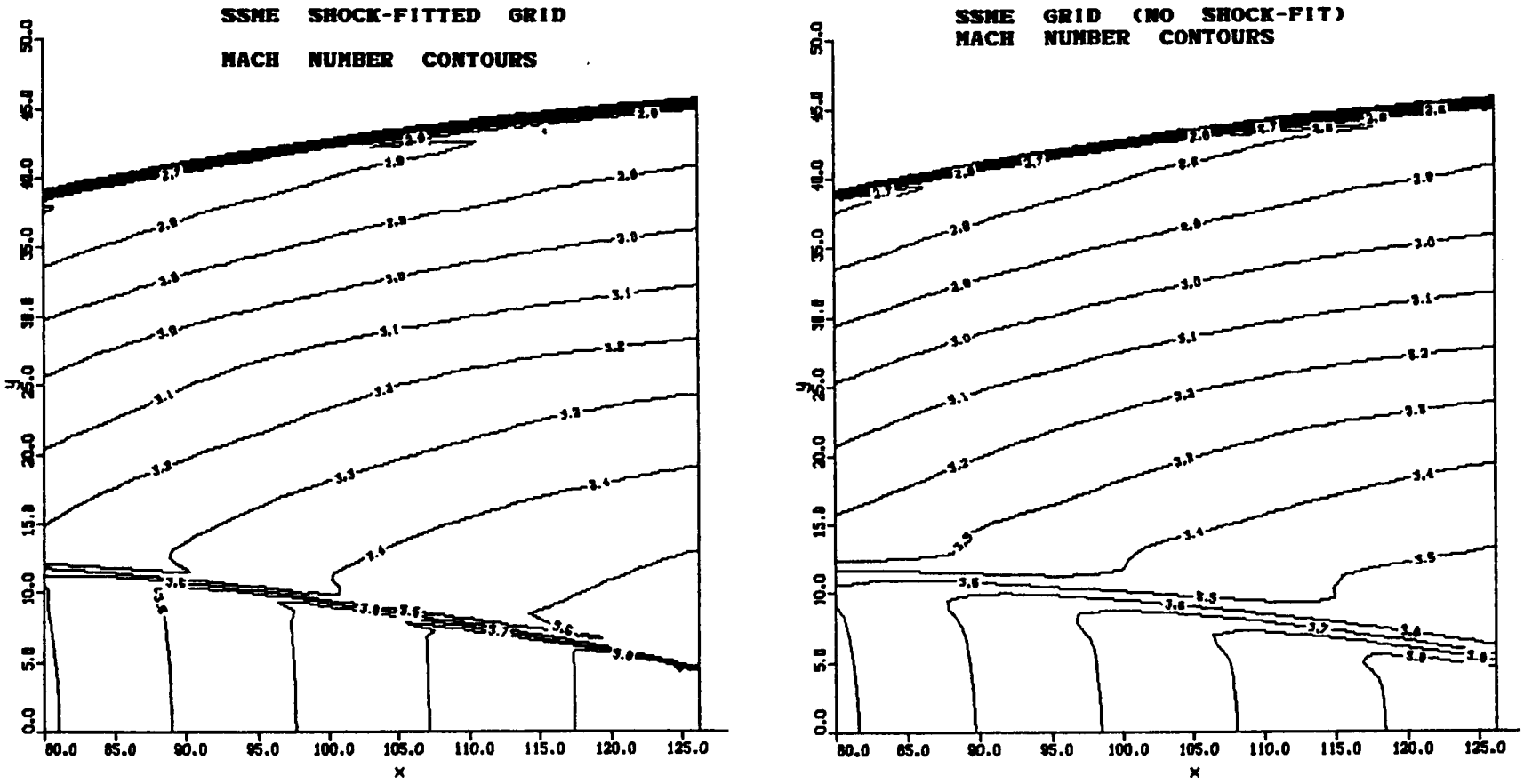


Figure 6. Shock-Capturing Grid Comparison.

better with the ideal values than for the Case 1 grid. This improvement was attributed to the grid packing along the shock in the Case 2 grid. The influence of the shock was now confined to a smaller portion of the over-all nozzle area. The inviscid Case 2 Mach number distributions along the wall and centerline did not change from the original Case 1 inviscid calculations or the Rocketdyne data.

One disadvantage of using the Case 2 grid for laminar calculations was that the level of convergence based on the convergence statistics of the PARC code (See Appendix A) was less than the level for inviscid calculations on the same grid. An L2 level of 10E-10 was achieved for the Case 2 inviscid solution, but only an L2 of 10E-4 for the laminar solution. Analysis of the calculations during the convergence process revealed that although the core of the nozzle flow was converging, the flow properties near the wall were constantly fluctuating, thus stalling the convergence of the solution at a relatively high L2 value. Every 500 iterations seemed to result in different profiles of temperature, pressure, and Mach number within the boundary layer. Varying the amount of artificial dissipation and changing the time step did not seem to solve the problem. It was concluded that the grid packing towards the wall was the source of the convergence problem.

A simplified grid called Case 3 was created to use for the laminar calculations with the intent of resolving the convergence problem. The grid packing was removed along the shock and reduced the packing towards the nozzle wall. In terms of packing towards the wall, the Case 3 grid had 13 grid points in the boundary layer region (defined for convenience as 98% of nozzle radius) at the nozzle exit plane while the Case 2 grid had 20 grid points in the same region. The Case 3 grid could be viewed as a compromise between the Case 1 and Case 2 grids.

It was possible to converge the Case 3 laminar flow field solution to the same level as the inviscid solutions (L2 of 10E-10). The same convergence problems as the previous laminar calculations were not experienced on the Case 3 grid. The time step (DTCAP) was the only variable that was changed during the convergence process.

The success of the Case 3 convergence led to another try at repacking the grid towards the wall again. The resulting Case 4 grid (again with no packing along the shock) had 24 grid points within the boundary layer region at the exit plane. Unfortunately, the Case 4 grid solution could not be converged to the level of the Case 3 grid.

At this point the experiments with grid packing within the boundary layer were stopped and the influence of artificial dissipation upon the flow field calculations was investigated.

The central-difference nature of the numerics of the PARC code requires the addition of artificial dissipation. Artificial dissipation acts similar to a fluid's viscosity. It dampens gradients within the flow field calculations which are induced by either the physics of the flow or from the numerics of the calculations. An example of how artificial dissipation can affect a numerical solution (in this case a step function) is shown in Figure 7. Note in the figure how the oscillations of the solution are damped with the addition of artificial dissipation. The step function in this example can represent pressure, density, etc., in the vicinity of a shock or boundary layer edge. The three major functions of artificial dissipation within the PARC code are: to stabilize the numerical calculations, dampen oscillations near discontinuities, and to enhance shock capturing [8,11].

The PARC code incorporates two artificial dissipation parameters, an explicit fourth order term (DIS4) and an implicit second order term (DIS2). DIS4 is uniformly applied throughout the computational domain. DIS2 is

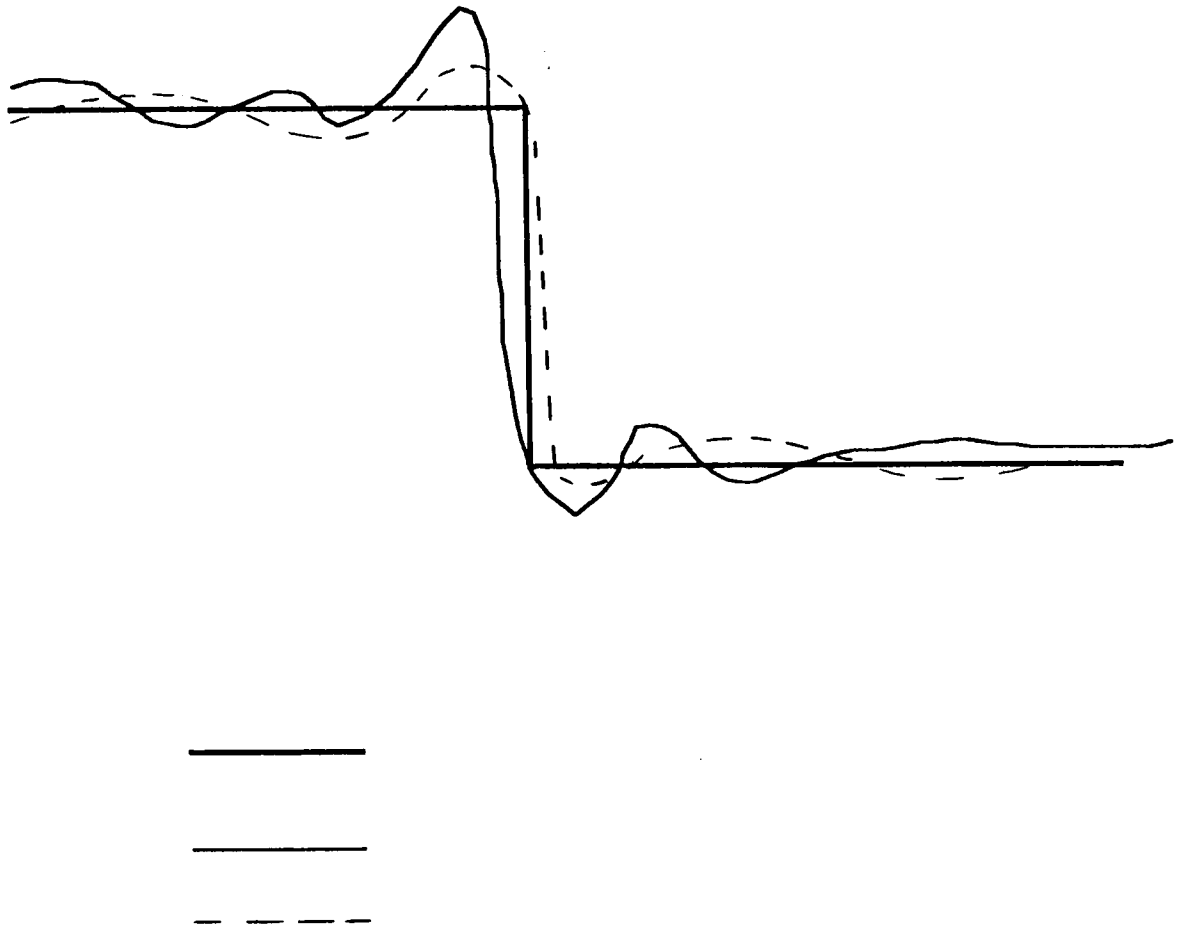


Figure 7. Effect of Artificial Dissipation on Solution.

activated only in regions of large pressure gradients; for example, shocks, compressions, and expansions. Artificial dissipation can objectionably combine with, or predominate over, a fluid's physical viscosity if not handled properly. This could result in erroneous flow field solutions.

All laminar flow field solutions except one were calculated with the latest PARC code, one with an improved artificial dissipation model. The remaining laminar solution was calculated using an enhanced artificial dissipation model incorporated within an earlier version of the PARC code.

The improved artificial dissipation model limits the amount of artificial dissipation used in the numerics of the code. The amount of dissipation is a function of the grid cell Reynolds number. Low cell Reynolds numbers resulted in a decrease in the amount of dissipation. For example, in the nozzle calculations, as one approaches the wall through the boundary layer the velocities and therefore the cell Reynolds numbers are decreasing, resulting in less artificial dissipation in the calculations. A comparison of the old and improved PARC artificial dissipation models is included in reference [13]. A thorough description of artificial dissipation within the PARC code can be found in reference [8].

An existing enhanced artificial dissipation model (EADM) was incorporated into the PARC version without the improved artificial dissipation. The model was created by Dr. Peter Liver from the Remtech Company, Huntsville, Alabama. The description of the EADM model is similar to that of the improved PARC model. The EADM model reduces the artificial viscosity in the calculations as the nozzle wall is approached. Again, this allows the physical viscosity of the fluid to predominate within the boundary layer. The difference between the improved PARC model and the EADM model was that the EADM was applied in the radial direction from a designated location in the computational grid to the nozzle wall. The EADM was not dependent upon the cell Reynolds number. A position of 75% of the nozzle radius from the centerline was chosen for the initiation of the EADM.

The EADM model was applied to the non-converged Case 2 grid. The results of the EADM experiments were that using EADM improved the convergence level of the Case 2 flow field solution. The same level of convergence (L2=10E-10) as the inviscid solution was attained with the EADM. The fluctuation of boundary layer profiles with iteration was not experienced. The convergence procedures were similar to earlier solutions. The only variable that was changed during the convergence process was DTCAP.

The results of the experiment were interesting. It was assumed that the Case 2 convergence level had stalled due to the computational grid. The convergence problem now appeared to be related to artificial dissipation, not to the computational grid. This example demonstrates the complexity of problems encountered when using CFD codes.

At this point the laminar flow field solutions will be summarized. Three different computational grids were used: Case 2, Case 3, and Case 4. Also, an enhanced artificial dissipation model was incorporated into the old PARC code and applied to the Case 2 solution. The total number of laminar solutions was four. The question is; which of the four flow field solutions gives the best results?

Each of the four solutions were compared qualitatively to a Blasius-type solution for compressible laminar flow over a flat plate [15,16]. The comparisons were performed at the exit plane for convenience. Using the Blasius solution for the analysis was justified by the condition of the flow in the exit plane region. The radius of longitudinal curvature is very large (essentially a flat plate) compared to the boundary layer thickness over the majority of the nozzle length. The pressure gradient across the boundary layer was roughly 2% at the exit. The velocity was nearly axial in the exit

plane region. Plots of velocity profiles for the different laminar PARC solutions are included in Figure 8.

The boundary layer velocity profiles in Figure 8 show that the Case 3 solution had the best comparison to a flat plate solution. The linear profile in the region near the wall and the transition from the linear to parabolic shape at a y/δ value of approximately .6 were expected trends for a flat plate. Both Case 2 plots resemble curves for a flat plate with a slight favorable pressure gradient.

A few general comments can be made about the plots in Figure 8. The plots show the tendency for all the laminar solutions to merge together at the edge of the boundary layer to the free stream conditions. All solutions predict approximately the same boundary layer thickness at the exit plane. Although no comparison is presented here, all solutions gave the same free-stream conditions. The most important observation from the plots is that each solution has slightly different boundary layer profiles.

The boundary layer temperature profiles in Figure 9 show a dependence on the computational grid and artificial dissipation. Note the discrepency in the wall temperature for each case. The ideal adiabatic wall temperature can be approximated from the following equation:

$$T_{aw} = T_o \left(\frac{1 + \frac{1}{2}(\gamma - 1) Pr^{\frac{1}{3}} M^2}{1 + \frac{1}{2}(\gamma - 1) M^2} \right) = 5953\ ^{\circ}R$$

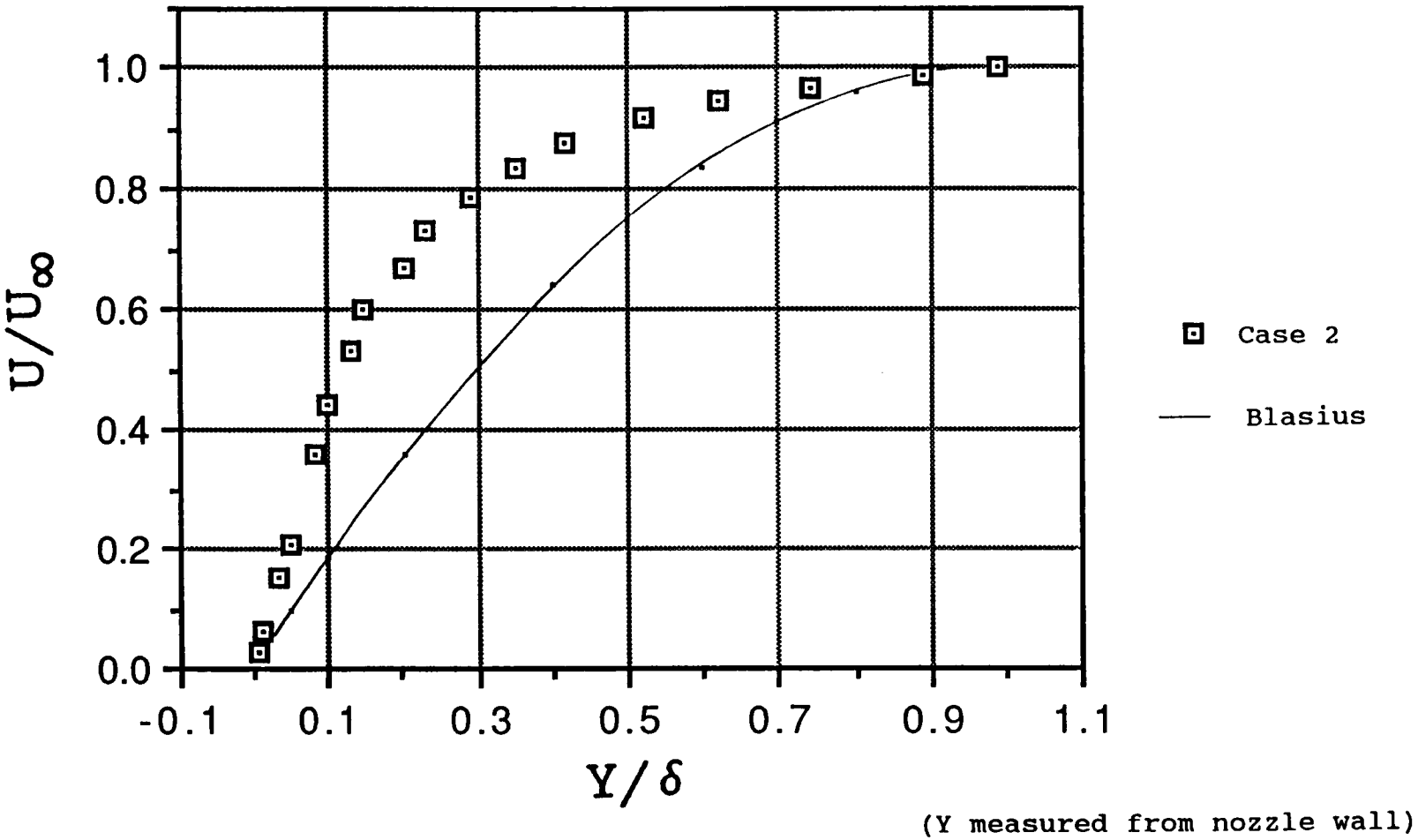


Figure 8. Laminar Boundary Layer Velocity Profiles.

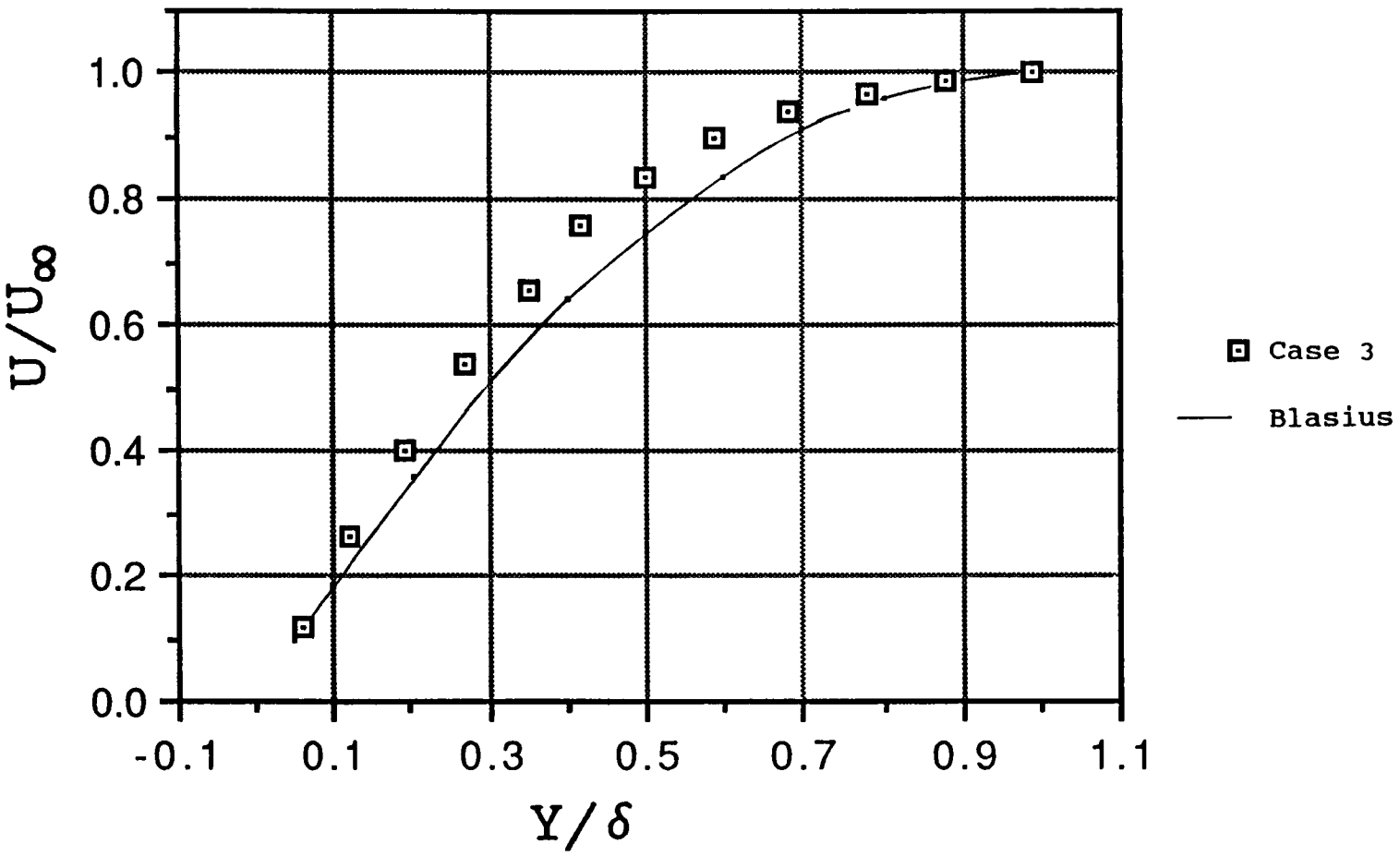


Figure 8. (Continued)

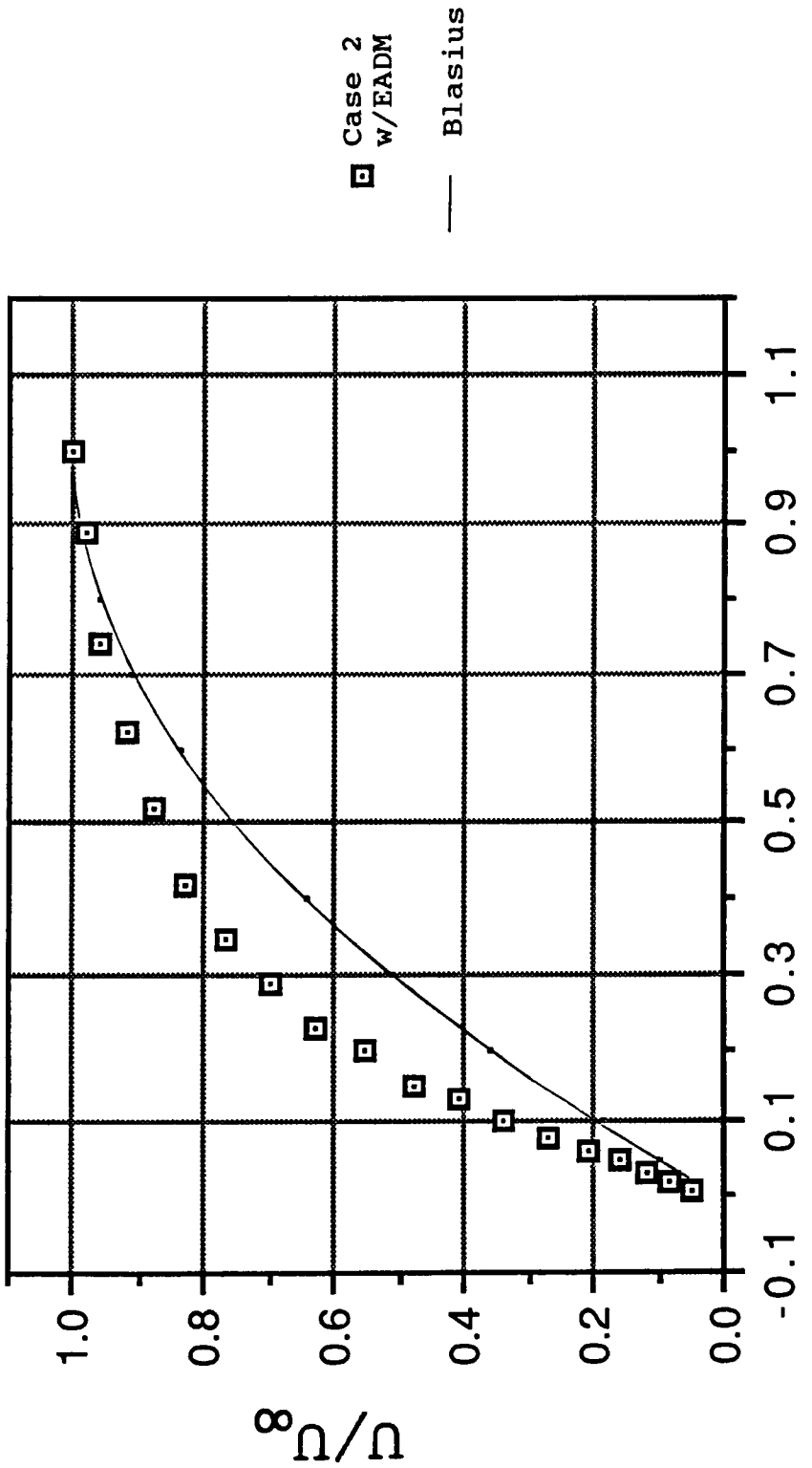


Figure 8. (Continued)

where,

T_{aw} = ideal adiabatic wall temperature,

Pr = Prandtl number,

T_o = nozzle chamber total temperature,

M = Mach number at boundary layer edge (4.253),

γ = ratio of specific heats.

The list of adiabatic wall temperatures calculated by the PARC code at the nozzle exit plane for the various laminar solutions were:

- Case 2.....4904 ^{o} R,
- Case 2 with EADM.....5664 ^{o} R,
- Case 3.....5490 ^{o} R,
- Case 4.....4393 ^{o} R.

Case 3 and Case 2 with EADM had the best correlation with the adiabatic wall temperature (within 8%). The slope of the temperature profile near the wall for the Case 2 with EADM is much steeper than the Case 2 or Case 3 slopes. The steep slope indicates an unrealistic abundance of heat loss in the wall region. The EADM was without doubt the source of the erroneous profile. Remember, the EADM is applied from a designated location in the radial direction. The EADM was not experimented with to see if the temperature profiles changed with the application location or by varying the amount of artificial damping within the EADM model.

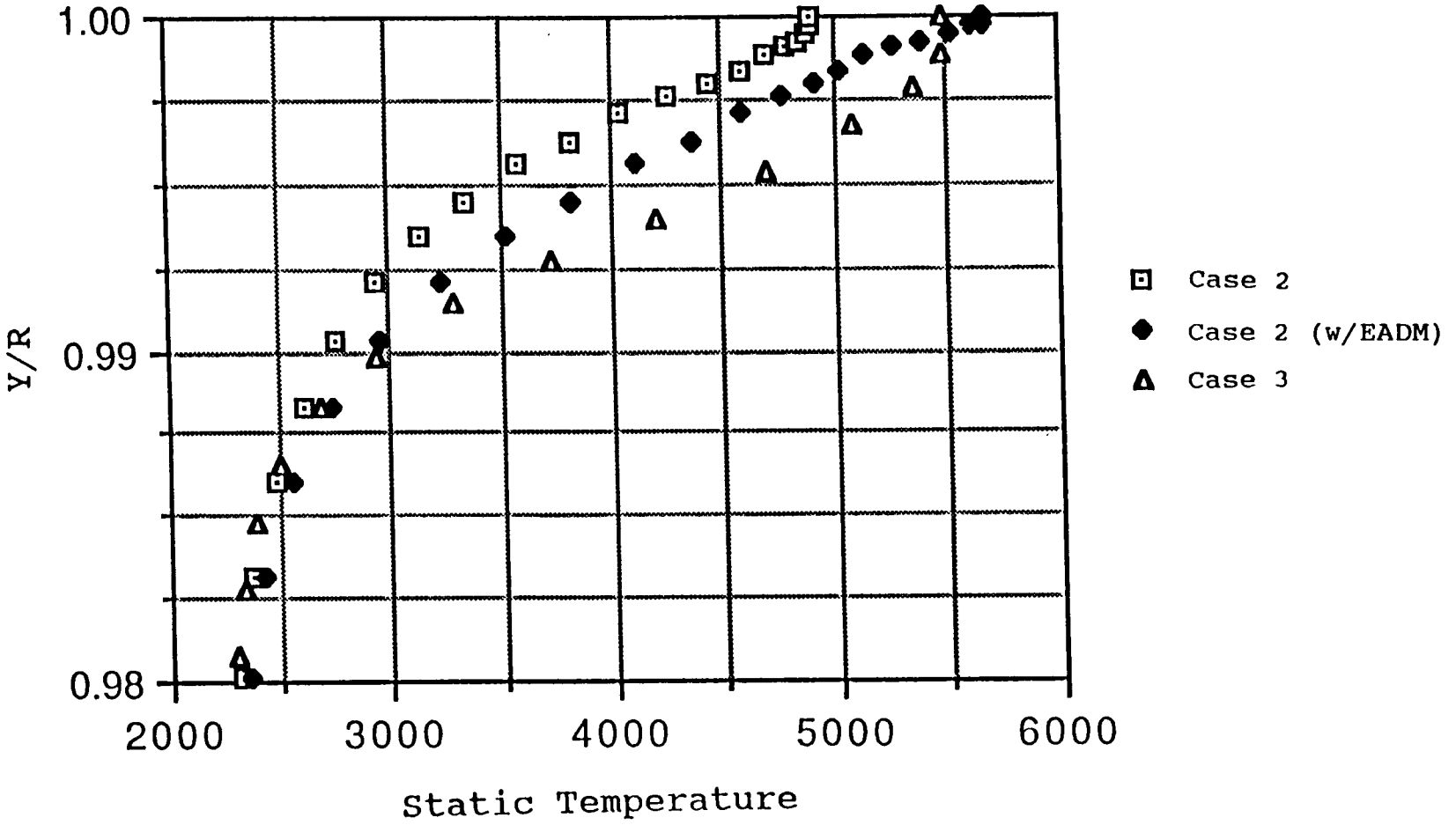


Figure 9. Laminar Boundary Layer Temperature Profiles.

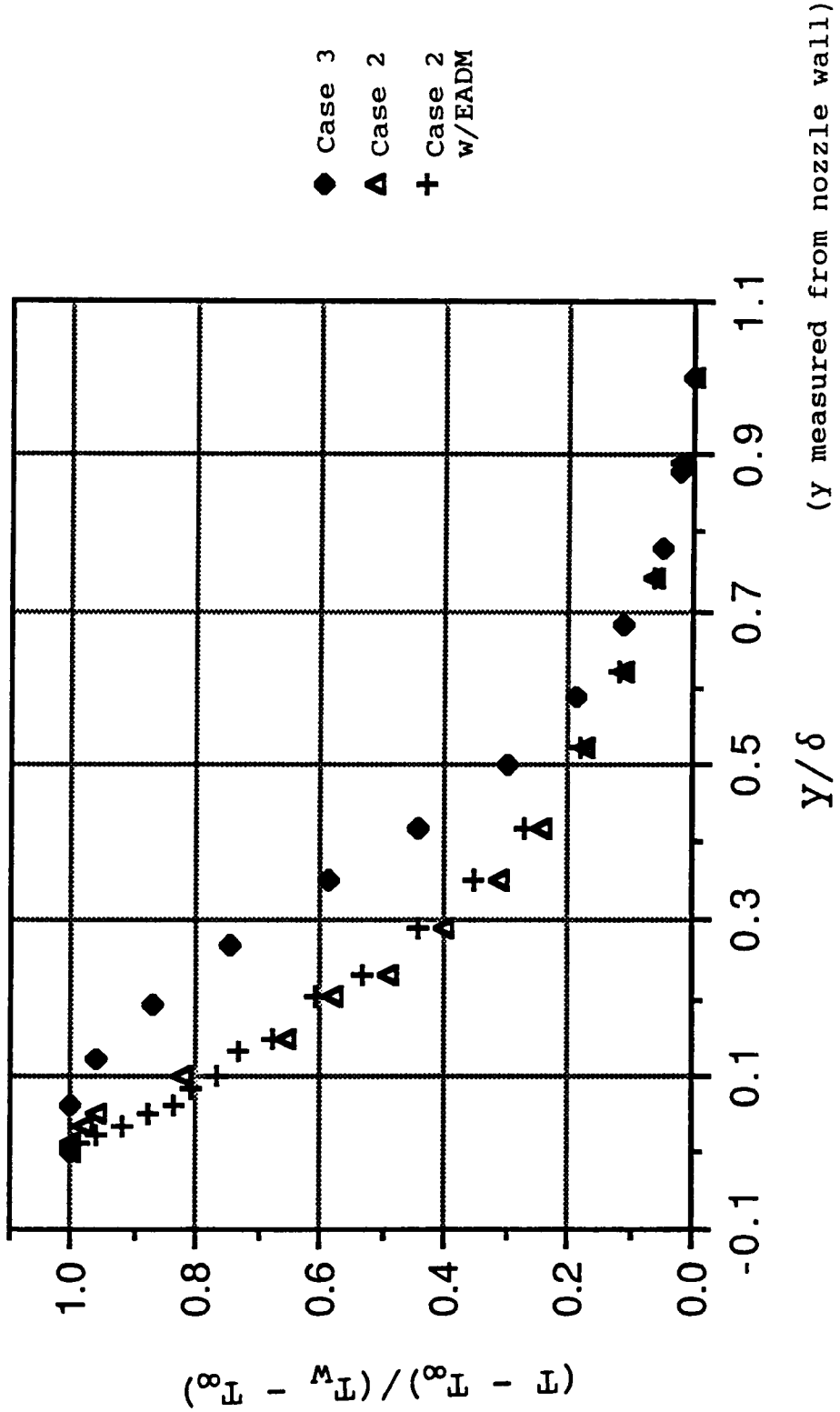


Figure 9. (Continued)

The varying temperature profiles signify a potential problem when calculating heat fluxes at the nozzle wall. Since the nozzle wall was adiabatic for these calculations The heat flux issue was not pursued further. This is an area for future investigation.

Calculation of the performance parameters for all laminar solutions are summarized in Table IV-1. The table shows that the performance levels did not vary from solution to solution even though all had different temperature, pressure, and Mach number profiles within their boundary layers. This observation is important because it demonstrates the robustness of the PARC code. Although each laminar solution was generated uniquely in terms of grid, artificial dissipation, and convergence, the resulting nozzle performance levels were similar.

Table IV-1. Laminar Performance Parameters

	m (lb/s)	F (x10E+5 lb_f)	Isp (sec)
Ideal	1223.5	5.077	424.4
Case 2	1209.0	4.732	391.4
Case 3	1218.0	4.770	391.5
Case 4	1216.0	4.764	391.8
Case 2 (w/EADM)	1215.0	4.754	391.3

Performing a statistical error analysis [24] on the performance levels for the different laminar solutions demonstrates the validity of using the PARC code for nozzle performance calculations. Comparing the average of the PARC laminar solution mass flows to the ideal mass flow value reveals a bias of -1.2%. The standard deviation of the PARC mass flows is .28%. Therefore, the uncertainty in the PARC laminar mass flow calculations is 1.3%. The statistical error equations are defined below:

$$\text{Average Bias} = B = \left(\frac{1}{n}\right) \sum_{i=1}^{n} [(\phi - \phi_i)/\phi_i]$$

$$\text{Std. Dev.} = S = \left((1/n) \sum_{i=1}^{n} [(\phi_{avg} - \phi)/\phi_{avg}]^2 \right)^{1/2}$$

Uncertainty = U = B + 2S

where,

ϕ = variable of interest (mass flow),

ϕ_{avg} = average value of the variable of interest (1214.5 lb_m/s),

n = number of cases (4).

The comparison between the average PARC mass flow and the ideal mass flow can be improved if the nozzle discharge coefficient is included in the ideal mass flow equation (See Appendix C). Using an estimated nozzle discharge coefficent of .9975 lowers the apparent PARC mass flow bias to -.75%.

The standard deviation of the thrust and specific impulse values from the PARC solutions are .3% and .06% respectively. Including these values with the mass flow analysis demonstrates the precision of the PARC code for nozzle performance calculations.

Comparing the laminar PARC performance values to the inviscid PARC levels shows good agreement. The average laminar flow rate is within .4% of the inviscid value. The PARC laminar specific impulse is slightly lower than

the inviscid level. The slightly lower level was expected due to the relatively thin laminar boundary layer.

Summarizing the laminar PARC solutions shows that the boundary layer profiles are a function of the computational grid and artificial dissipation. Because the boundary layer was relatively thin for the SSME nozzle, the effect of the various boundary layer profiles on the over-all nozzle performance was minimal, as demonstrated by the similar nozzle performance levels for the different test cases.

CHAPTER V

TURBULENT CALCULATIONS

The objective of the turbulent calculations was to compare PARC flow field solutions to the PARC inviscid and laminar flow field solutions and to theoretical calculations. Only one turbulent flow field calculation on one grid was made for this research. The experience gained from the laminar calculations was used to eliminate most of the trial-and-error process of generating a flow field solution. Validation of the turbulent calculations was dependent on how well the data compared to the theoretical calculations and to the other flow field solutions.

A new grid was created for the turbulent calculations. The new grid had the shock-fitted and sonic line features of previous grids. The number of grid points in the radial direction was increased from 100 to 120. The grid was very tightly packed towards the wall along the entire nozzle length. A hyperbolic stretching function in the INGRID code was used to pack the grid in the radial direction towards the wall. Approximately 25 grid points were located within the boundary layer along the nozzle length.

The PARC code utilizes the Baldwin-Lomax algebraic two-layer eddy viscosity turbulence model [23]. The

origins of this model are the Prandtl-Van Driest formulation for the inner layer, and the modified Clauser approximation for the outer layer [15,16]. Comparisons of results by other researchers show that this model agrees with either experimental data or other creditable boundary layer codes . The model also has been demonstrated to adequately express shock-boundary layer interactions on a flat plate [13,23].

The PARC code couples its turbulence model with the thin-layer approximation for the Navier-Stokes equations. The turbulence model was applied in the direction normal to the flow (radial direction) only. However, the viscosity terms were retained in both the stream-wise and radial directions. The PARC inputs for this arrangement are described in Appendix A.

The turbulent convergence process was started by using the laminar inputs to the PARC code for the first 3000 iterations. After iteration 3000 the inputs were switched to the turbulent values. The turbulent inputs were used for the remainder of the iteration sessions.

The purpose of using the laminar inputs initially was to prevent the solution from stalling before the flow field was established. The complexity of the turbulent Navier-Stokes equations and the density of the computational grid within the boundary layer could have limited

the level of convergence (L2) to a point magnitudes less than the laminar and inviscid solutions.

During the actual convergence process the convergence statistics started to oscillate around the L2 level of 10E-4 after 6000 iterations. The L2 was reduced to 10E-5 by lowering the time-step (DTCAP). Eventually, the solution oscillated about the new L2 level. Lowering DTCAP or changing the other convergence parameters failed to lower L2 further.

The boundary layer profiles of temperature, pressure, and Mach number from the PARC code's interactive output file (IOF) were used to monitor the progress of the solution. After 15,000 iterations the profiles had not changed significantly from the previous iteration session. Therefore the convergence process was stopped. See Appendix A for a complete discussion of the convergence procedures.

To gain confidence in the turbulent boundary layer solution I extracted the friction velocity parameter (u^+) from the turbulence subroutines in the PARC code. A good correlation between the extracted values and the empirical relations indicated solution convergence. I used Spalding's composite law equation [15] to correlate the friction velocity to the transverse distance parameter (y^+):

$$y^+ = u^+ + e^{-kB} [e^{ku+} - 1 - ku^+ - (ku^+)^2/2 - (ku^+)^3/6]$$

where;

u^+ = ratio of mean velocity to friction velocity,

y^+ = transverse coordinate for the law of the wall,

$k = .41$,

$B = 5.0$.

Figure 10 shows the plot of of u^+ and y^+ at the exit plane. The results show that there were enough grid points within the sublayer (y^+ less than 10) and the near-wall region to adequately resolve the turbulent boundary layer.

The adiabatic wall temperature calculated by the PARC code was much less than the expected temperature. As an example, at the exit plane, the expected adiabatic wall temperature was calculated as:

$$T_{aw} = T_o \left(\frac{1 + \frac{1}{2}(\gamma - 1) Pr^{1/3} M^2}{1 + \frac{1}{2}(\gamma - 1) M^2} \right) = 6453\ ^{o}R$$

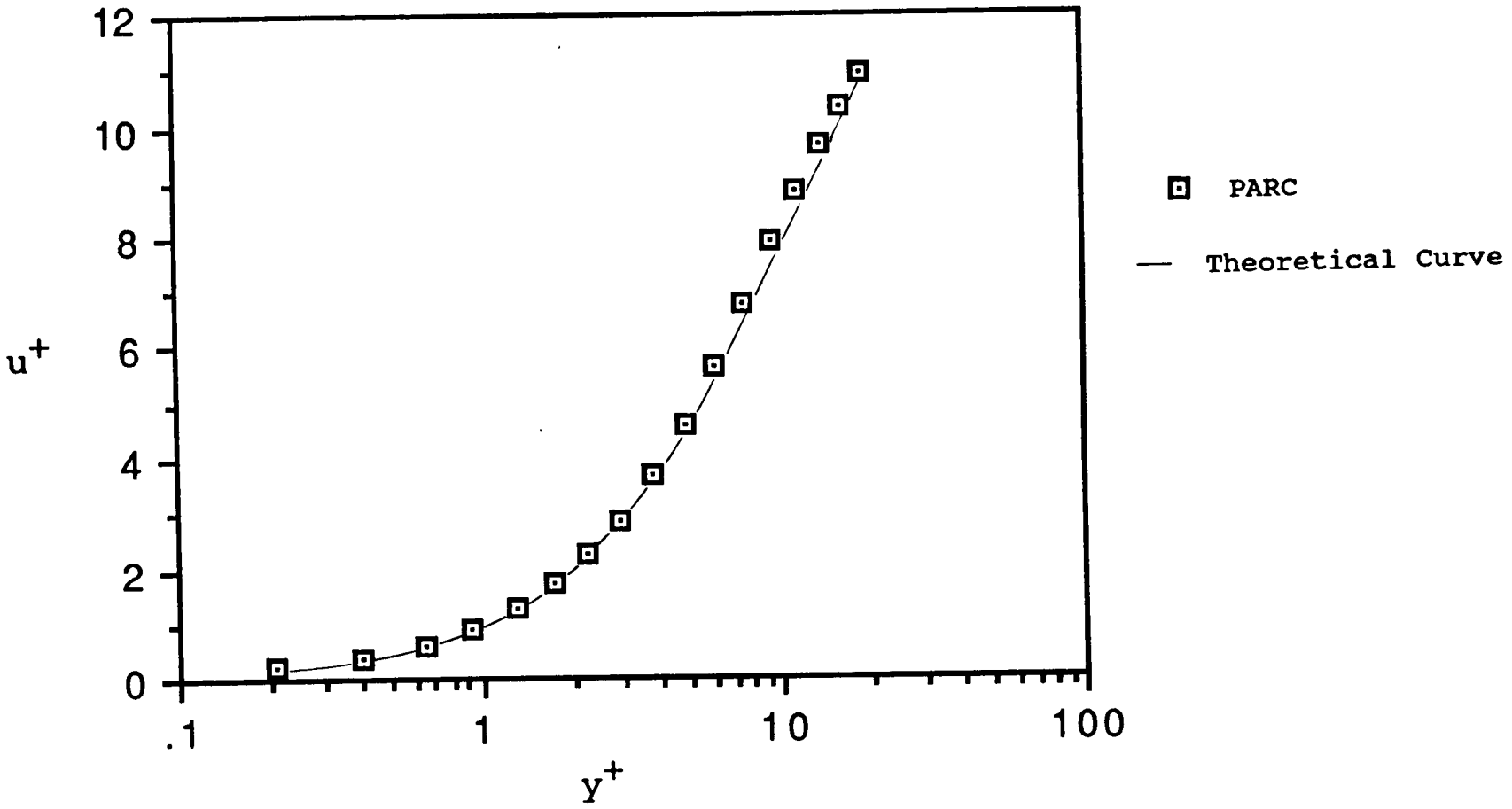


Figure 10. Law of the Wall Parameters.

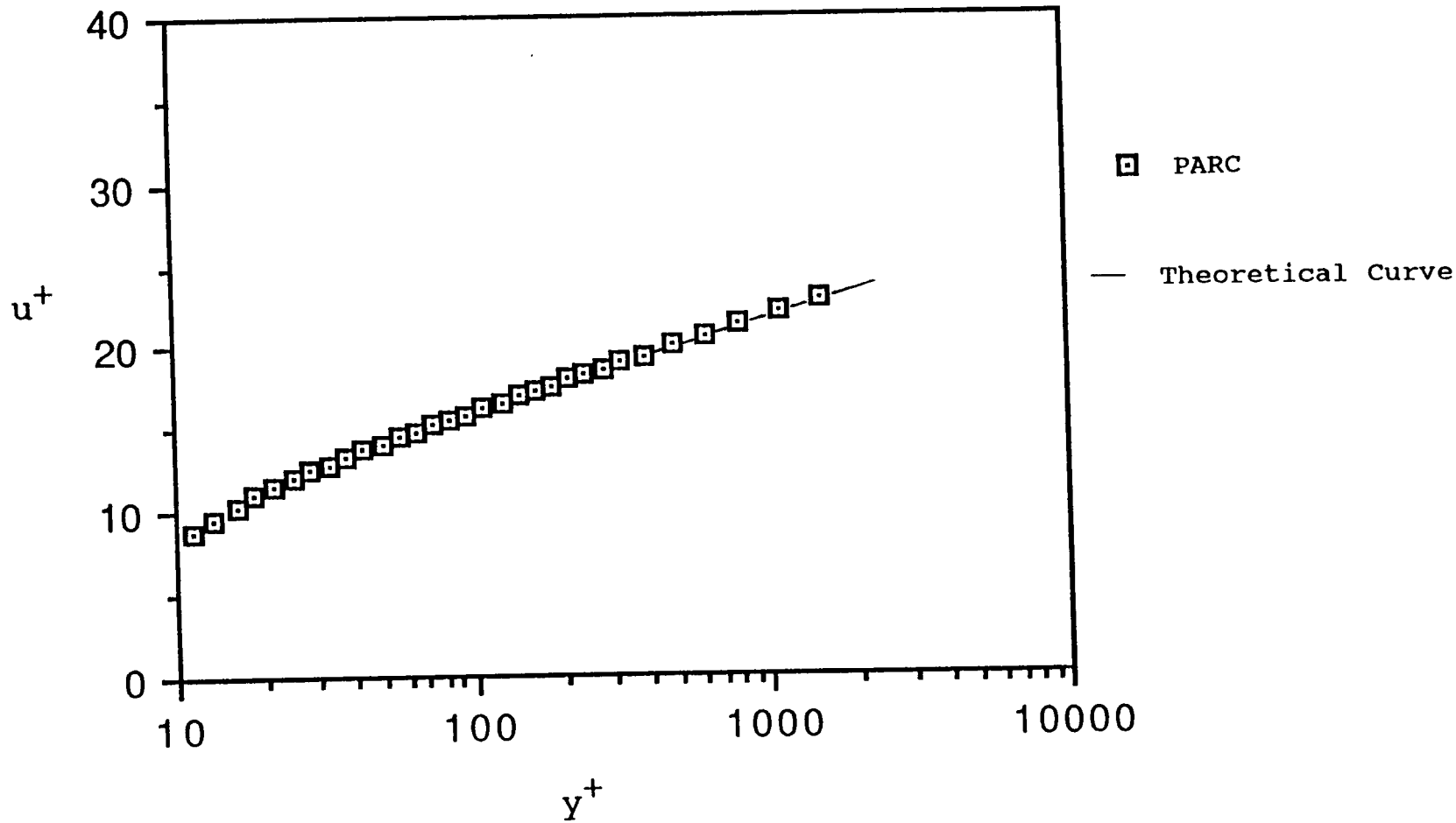


Figure 10. (Continued)

where,

T_{aw} = ideal adiabatic wall temperature

T_o = nozzle chamber total temperature,

Pr = turbulent Prandtl number,

M = Mach number at the boundary layer edge,

γ = ratio of specific heats.

The wall temperatures calculated by the PARC code were lower than expected. The negative temperature bias was on the order of 25%, larger than the bias for the laminar solutions. The laminar solutions that converged completely (Case 3 and Case 2 with EADM) were closer to the expected wall temperatures than the solutions that didn't converge completely (Case 2 and Case 4). This could be an indication that the turbulent solution had not converged completely near the wall. Decreasing the grid density within the boundary layer or applying the EADM to the turbulent calculations are two methods which could improve the wall temperature calculation. These methods could also enhance the convergence of the turbulent solution, as discussed in the Laminar Calculation chapter.

Comparing the turbulent boundary layer profiles to those from the laminar calculations helps to validate the turbulent calculations. Case 3 was chosen to

represent the laminar calculations. The comparisons are of a qualitative essence because neither experimental data, nor data generated by a proven boundary layer code, were available.

Figure 11 is a comparison of the nondimensional temperature parameter within the boundary layers. Although it was determined from the previous discussion that the turbulent wall temperature was much lower than expected, Figure 11 shows that the shape of the temperature curve through the boundary layer appears to be correct. As expected, the curve is very steep near the wall. It was also expected that the turbulent profile would be below the laminar profile as the plot indicates [13,15,16].

Figure 12 is a comparison between the laminar and turbulent boundary layer nondimensional velocity profiles. The comments for the velocity profile are similar to those for the temperature profile. The steepness of the turbulent curve near the wall and the transition in the shape of the turbulent curve at the Y/δ value of .1 were expected characteristics.

An analysis of the turbulent boundary calculations based on the momentum integral methods of Prandtl and Blasius was also performed [15,25,26]. The objective of this analysis was to compare the boundary layer growth using an integral analysis to the boundary layer growth

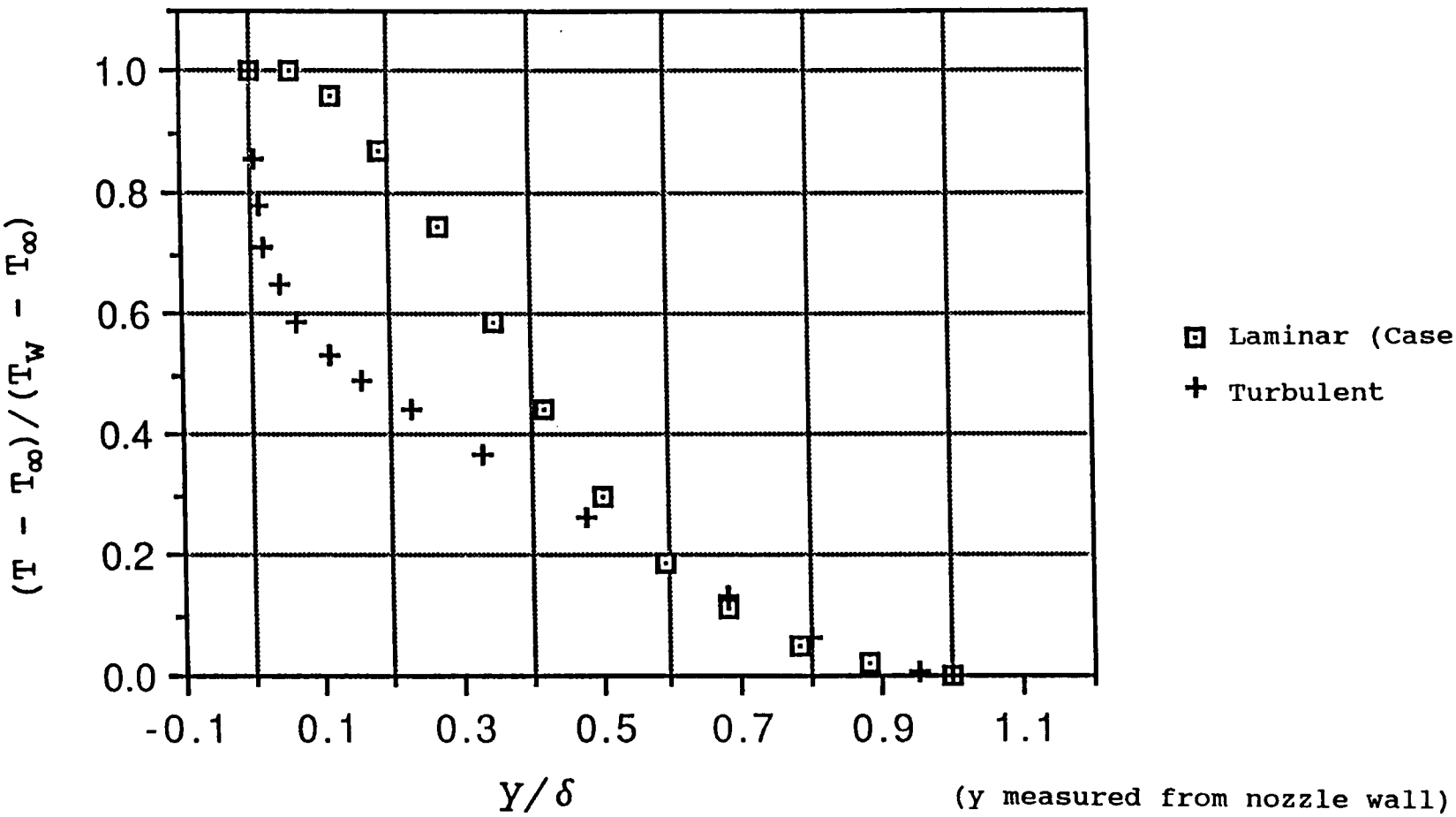


Figure 11. Boundary Layer Temperature Profile Comparison.

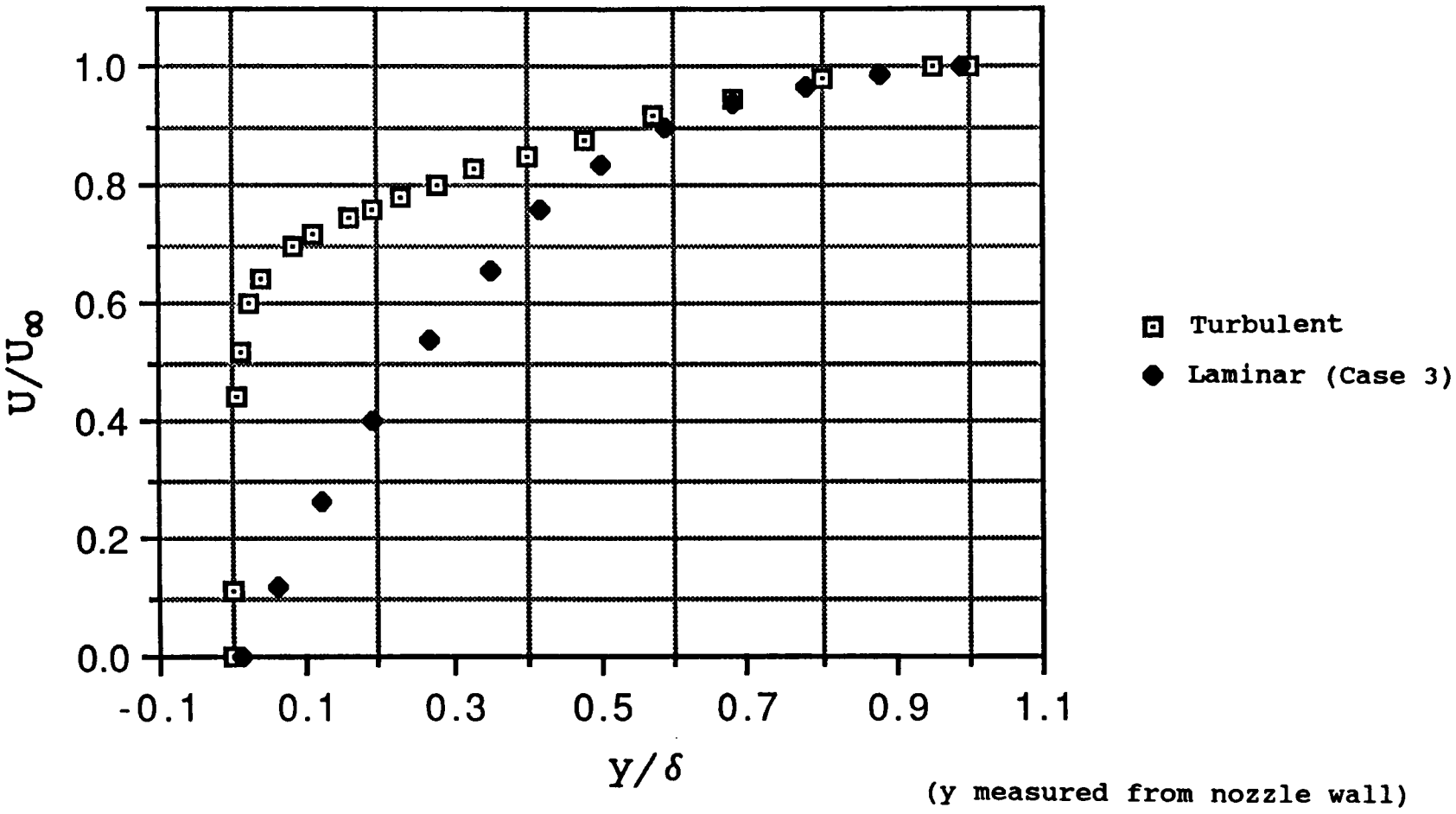


Figure 12. Boundary Layer Velocity Profile Comparison.

indicated by the PARC code solution. The calculations are summarized in Appendix C.

A section of nozzle length was chosen for analysis close to the nozzle exit to simulate a flat plate condition. The boundary layer growth along the section was calculated and compared to the PARC results. The nozzle section chosen was essentially flat and had a favorable pressure gradient along its length. Tables of data from [26] simplified the integral analysis by reducing the calculations to an algebraic exercise.

The reason the relative boundary layer growth approach was taken instead of trying to calculate the actual boundary layer growth along the entire nozzle length was the complexity of such an analysis. The fluctuating wall curvature, possible relaminarization, and shock-boundary layer interaction makes an absolute boundary layer growth analysis difficult.

The geometrical nozzle throat plane was used as the datum to locate the coordinates of the wall section. The wall section was defined as the distance along the wall between the x=100.6" and x=121.2" locations, x measured from the datum.

The assumptions for the momentum integral analysis were that the data tabulated in [26] for a gamma of 1.4 were valid for the gamma of 1.2 for this application.

The static pressure fluctuation through the boundary layer in the PARC solution (roughly 5%) was also assumed to have no impact on the analysis.

The comparison of results for the turbulent PARC solution and the momentum integral method were:

$\Delta\delta_{PARC}$ = .554 inch,

$\Delta\delta_{CALC}$ = .576 inch.

The results show that both methods are in good agreement for the boundary layer growth over the nozzle wall section. The oscillation in the PARC solution in the vicinity of the boundary layer edge complicated the process of extracting the boundary layer thickness from the PARC data. Nonetheless, the comparison shows that the boundary layer thickness extracted from the PARC turbulent flow field solution was of the correct magnitude.

A comparison between the boundary layer thickness at the nozzle exit plane for the turbulent PARC solution and the laminar PARC solution (Case 3) shows that the thickness for the turbulent case is nearly four times the laminar thickness:

δ_{turb} = 2.751 inch

δ_{lam} = 0.78 inch

The performance calculations for the turbulent flow field calculations were calculated and compared to the

performance levels for the inviscid and laminar calculations. Below are the turbulent performance levels:

Mass Flow (m) = 1220.0 lb_m/s,

Thrust (F) = 472,400 lb_f,

Specific Impulse(Isp) = 387.3 s .

Comparing the above levels to those in Tables III-1 on page 20 and IV-1 on page 43 show good correlation. The turbulent mass flow value is within the uncertainty bandwidth established by the multiple inviscid and laminar mass flow calculations. The turbulent specific impulse value completes the trend of decreasing specific impulse level with increasing boundary layer thickness.

CHAPTER VI

CONCLUSIONS

The results from the inviscid flow field calculations show that the PARC solution is in good agreement with the results from Rocketdyne. Results for the Mach number distributions along the wall and centerline were essentially equal. The worst deviation occurred along the centerline at the nozzle exit, where the calculated Mach numbers differed by only .4%. The good correlation between the PARC results and the baseline data set from Rocketdyne demonstrates the ability of the PARC code to calculate inviscid flow field solutions in the SSME rocket nozzle.

Creating viscous flow field results with the PARC code revealed some of the limitations of CFD code calculations in general. It was demonstrated that the flow properties within the nozzle boundary layers were dependent on the computational grid, the solution convergence process, and the amount of artificial dissipation within the numerics of the code. These variables created uncertainty regarding the results of the boundary layer flow calculations.

The laminar boundary layers calculated by the PARC code were relatively thin compared to the nozzle radius. The thinness of the boundary layers were expected due

to the high Reynolds numbers within the flow. Because the boundary layers were thin, it was found that the influence of the boundary layer on the over-all nozzle flow field was minimal.

The laminar flow field results from the PARC code compared well with expected trends and theoretical calculations. No laminar flow data was available from Rocketdyne for comparison. The laminar results also correlated well with both the inviscid and turbulent nozzle flow fields generated by the PARC code in terms of performance levels and flow field characteristics.

Observations on the PARC turbulent flow field results are similar to those for the laminar results. The turbulent results correlate well with the laminar calculations. The turbulent PARC results also compare well with expected theoretical trends and calculations.

The turbulent flow field results magnified a problem with the calculation of the adiabatic wall temperature; a problem which existed to a lesser extent in the laminar calculations. The PARC calculation of the turbulent adiabatic wall temperature along the nozzle length was low compared to the ideal value by as much as 25%. It was not determined if the negative bias was the result of the solution convergence process or if it was inherent to the

PARC code itself. Since heat transfer was not an interest for this study, the discrepency was not studied further. This problem is an area for future investigation.

The PARC code was modified during this investigation to calculate the nozzle performance parameters of mass flow, thrust, and specific impulse. Although absolute thrust levels were not obtainable with this PARC code, the relative thrust levels for the different flow field calculations as a group show the correct trend. For example, although the boundary layer growth between the inviscid and laminar solutions (and likewise between the laminar and turbulent solutions) was small, the momentum deficit within the boundary layers was detected by a slight decrease in the specific impulse levels of the solutions.

The statistical analysis of the performance levels calculated by the PARC code demonstrate the precision with which the PARC code can contribute as a nozzle performance predictor. Multiple PARC laminar solutions resulted in standard deviations in mass flow, thrust, and specific impulse calculations of .25%, .30%, and .06% respectively. Mass flow was the only PARC performance parameter which could be correlated to an ideal value. Comparison between the mass flows from the PARC solutions to the ideal mass flow rate revealed a bias of roughly -1% for the PARC code.

The PARC code could be a useful tool during the design phase of a rocket nozzle. The results of this research show that the PARC code is a versatile and precise CFD code in terms of flow field and performance parameter calculations. An example of an application of the PARC code within the design process would be the case of determining the thrust increment resulting from the alteration of the nozzle contour. The PARC code could minimize experimental testing of prototype nozzle designs by allowing the designer to determine flow characteristics and performance levels without building model hardware.

BIBLIOGRAPHY

BIBLIOGRAPHY

1. "JANNAF Rocket Engine Performance Prediction and Evaluation Manual," CPIA-PUBL-245, Chemical Propulsion Information Agency, Laural, MD, April, 1975.

2. Nickerson, G.R., Coats, D.E., and Dang, L.D., "Two-Dimensional Kinetic Reference Computer Program (TDK)," NASA CR-178628, 1985.

3. Coats,D.E. and Kehtarnavaz, H. "Effect of Transverse and Longitudinal Curvature on Nozzle Boundary Layer Growth," AIAA paper no. 87-1821, AIAA 23rd Joint Propulsion Conference, June 29-July 2, 1987.

4. Smith, T.A., Pavli,A.J., and Kacynski, K.J. "Comparison of Theoretical and Experimental Thrust Performance of a 1030:1 Area Ratio Rocket Nozzle at a Chamber Pressure of 2413 kN/m^2 (350 psia)," AIAA paper no. 87-2069, AIAA 23rd Joint Propulsion Conference, June 29-July 2, 1987.

5. Smith, T.A. "Boundary Layer Development as a Function of Chamber Pressure in the NASA Lewis 1030:1 Area Ratio Rocket Nozzle," AIAA paper no. 88-3301, AIAA 24th Joint Propulsion Conference, July 11-13, 1988.

6. Davidian, K.J., "Comparison of Two Procedures for Predicting Rocket Engine Nozzle Performance," AIAA paper no. 87-2071, AIAA 23rd Joint Propulsion Conference, June 29-July 2, 1987.

7. Collins, F.G., "Computation of Nozzle Flow Fields Using the PARC2D Navier-Stokes Code," Final Report of NASA/ASEE Summer Faculty Fellowship Program, in NASA CR-178966, November, 1988.

8. Pulliam, T.H. "Euler and Thin-Layer Navier Stokes Codes: ARC2D, ARC3D," Notes for UTSI Computational Fluid Dynamics Workshop, 1984.

9. Cooper, G.K. "The PARC Code: Theory and Usage," Arnold Engineering Development Center TR-87-24, Arnold Air Force Station, TN, October, 1987.

10. Dorrell, E.W., Jr., and Soni, B.K. "INGRID: Interactive Two-Dimensional Grid Generation," Arnold Engineering Development Center TR-86-49, Arnold Air Force Station, TN, February, 1987.

11. Anderson, D.A., Tannehill, J.C., and Pletcher, R.H. Computational Fluid Dynamics and Heat Transfer. Hemesphere Publishing Corporation, New York, 1984.

12. Dutton, J.C. and Addy, A.L. "Transonic Flow in the Throat Region of Axisymmetric Nozzles," AIAA Journal, vol. 19, no. 6, June 1981.

13. Cooper, G.K., Garrard, G.D., and Phares, W.J. "PARC Code Validation for Propulsion Flows," Arnold Engineering Development Center TR-88-32, Arnold Air Force Station, TN, January, 1989.

14. Liepman, H.W. and Roshko, A. Elements of Gas Dynamics John Wiley and Sons Inc., 1957.

15. White, F.M. Viscous Flow. McGraw-Hill Book Co., 1974.

16. Schetz,J.A. Foundations of Boundary Layer Theory. Prentice-Hall Inc., New Jersey, 1984.

17. Cheer, A.Y., Saleem, M., Pulliam, T.H., and Hafez, M. "Analysis of the Convergence History of flow through Nozzles with Shocks," AIAA paper no. 88-3795.

18. John, J.E.A. Gas Dynamics. Allyn and Bacon, Inc., 1984.

19. Cooper, G.K., Jordan, J.L., and Phares, W.J. "Analysis Tool for Application to Ground Testing of Highly Under-expanded Nozzles," AIAA paper no. 87-2015, AIAA 23rd Joint Propulsion Conference, June 29-July 2, 1987.

20. Thompson, J.F., Warsi, Z.U.A., and Mastin, C.W. Numerical Grid Generation: Foundations and Applications. North-Holland, 1985.

21. Eiseman, P.R. "Orthogonal Grid Generation," Numerical Grid Generation. North-Holland, 1982.

22. "EADS CRAY User's Guide," Document Number GDS-MSFC -002, Grumman Data Systems, NASA Marshall Space Fight Center, Huntsville, AL 1988.

23. Baldwin, B.S. and Lomax, H. "Thin Layer Approximation and Algebraic Model for Seperated Turbulent Flow," AIAA paper no. 78-257, AIAA 16th Aerospace Sciences Meeting, January 16-18, 1978.

24. Abernathy, R.B. and Thompson, J.W. "Handbook--Uncertainty in Gas Turbine Measurements," Arnold Engineering Development Center TR-73-5, Arnold Air Force Station, Tennessee, January 1973.

25. Smith, R.E. "A Theoretical Method of Determining Discharge Coefficients for Venturis Operating at Critical Flow Conditions." Master's Thesis, University of Tennessee Space Institute, December, 1962.

26. Tucker, M. "Approximate Turbulent Boundary Layer Development in Plane Compressible Flow Along Thermally Insulated Surfaces with Application to Supersonic-Tunnel Contour Correction." NACA paper no. TN 2045. March 1950.

APPENDIXES

APPENDIX A

COMPUTATION PROCEDURES

This appendix chronologically summarizes the procedures used to generate flow field solutions with the PARC code. The purpose of this summary is to document the steps used to generate flow field solutions for reference in this paper and for future follow-on work. The summary starts with the information needed to run the INGRID grid generation program and ends with the PARC output. The summary is not intended to reiterate the code manuals [9,10].

INGRID CODE

The first step before using the INGRID code was to divide the nozzle contour up into basic geometric segments or boundaries that could be handled by the INGRID code. The segments or boundaries for the nozzle fell into three catagories; straight sections, arcs of a circle, or spline fits. The coordinates for the SSME nozzle wall were provided by Rocketdyne. See Figure A-1 for a generic sketch of the nozzle segments.

The next step before running the INGRID code was to determine the quantity of grid points needed and how they should be distributed within the physical domain.

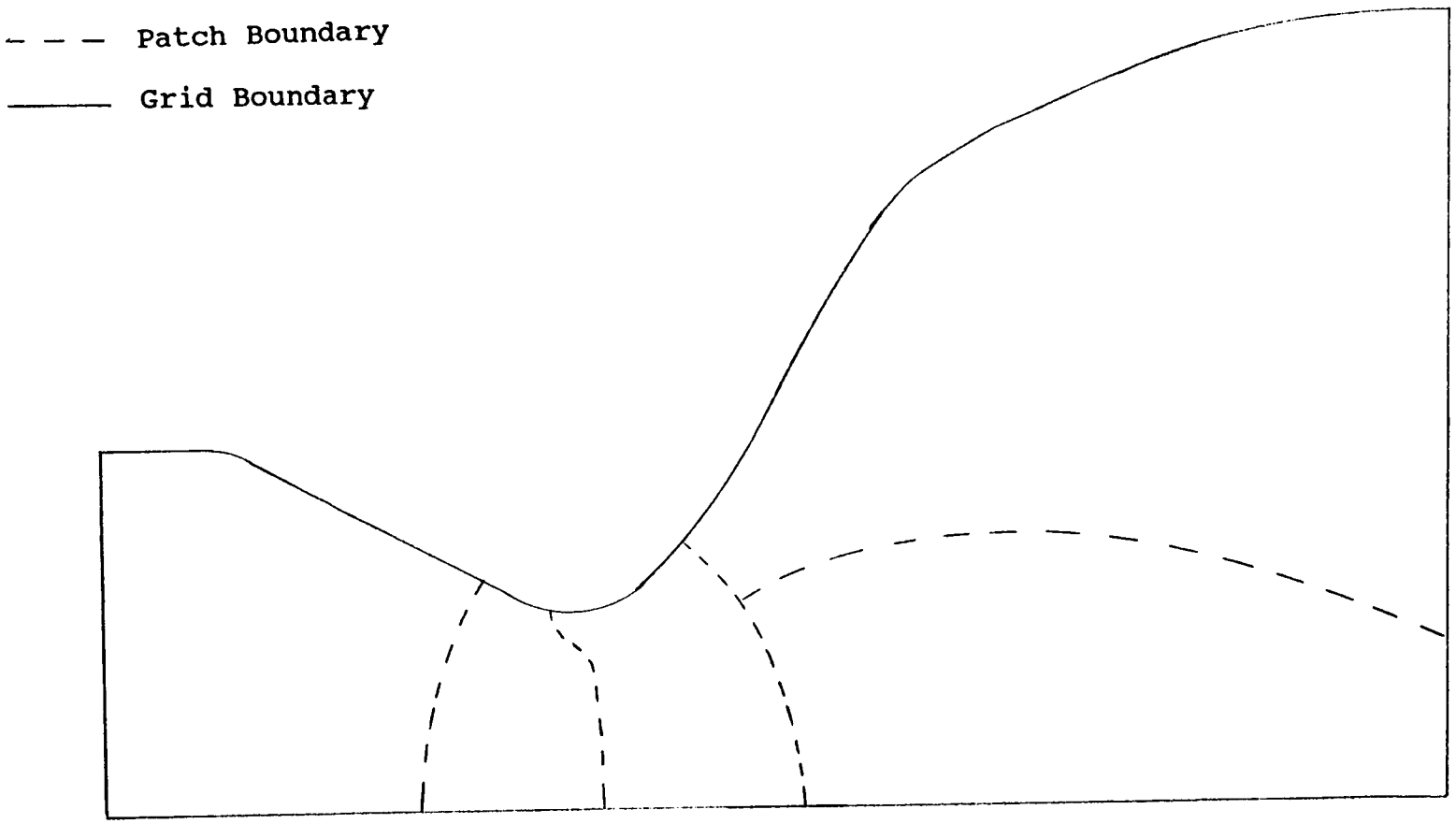


Figure A-1. Generic Sketch of Grid Boundaries and Patches.

Two hundred and ten (210) grid points were chosen for the axial direction and 100 points in the radial direction for both the inviscid and laminar calculations. The quantity was increased to 120 points in the radial direction for the turbulent boundary layer calculations. Basically, the quantities chosen were based on the experience of other PARC users for similar applications.

The grid points were distributed with the intent of concentrating the points in areas of large fluid property gradients. All grids were packed within the throat region of the nozzle to resolve the transonic flow region. All grids also had mild packing along the length of the nozzle centerline. The laminar and turbulent flow fields had wall-packing to resolve the boundary layers. The Case 2 grid had packing along the length of the embedded shock in the nozzle to improve the resolution of the shock.

The INGRID program runs interactively. The program input session consists of a series of questions which transform the physical nozzle space into the computational grid space. The questions are too numerous to list here. The questions, user-supplied answers, and the program reponses are written to a history file generated by the INGRID code. The history file can serve as the input file to the INGRID program to regenerate a grid. Any mistakes or additions to the input session can be made by editting the history file after the interactive INGRID program session.

The INGRID program allows the option of plotting the grid after the input session, assuming the terminal has the required graphics capability. Plotting the grid initiates the grid refinement process. The purpose of the refinement is to improve the quality of the initial grid. The following is a list of grid characteristics which were examined during refinement:

1. Distribution of grid points.
2. Grid skewness.
3. Grid orthogonality.
4. Uniform grid spacing.
5. Over-all grid smoothness.

These grid characteristics can be improved by either modifying the history file or using the grid refinement options within the INGRID code.

Grid orthogonality was an area that required extra refinement work for the SSME nozzle grid. Ideally, one would like the directional grid lines to be perpendicular (orthogonal) to each other and to the grid boundaries. The impetus for grid orthogonality was that grid <u>non-orthogonality</u> increases the computational truncation error associated with the grid. It also increases the computation time for a solution due to the presence of off-diagonal metric tensor terms in the numerics of the PARC code [20,21].

The changing curvature of the nozzle wall complicated the process of generating an orthogonal grid for the SSME nozzle. Implementing the orthogonal grid generation systems within the INGRID code was unsuccessful. The problem was circumvented by trying to introduce orthogonality into the grid via the boundary definitions. The nozzle interior grid domain was divided into patches. A patch is defined by a region enclosed by four boundaries. The advantage of using patches is the freedom to define the patch-enclosing boundaries as desired. See Figure A-1 for an example of how the grid was divided into five patches. Note from Figure A-1 that boundaries 2, 6, and 9 were defined to induce orthogonality at the nozzle walls for the grid lines within the patches. Viewing Figure 1 on page 11 and 12 shows that there is room for improvement in the implementation of grid orthogonality. The grids were not completey orthogonal.

Smoothing is the last grid refinement process to be implemented on the grid. Grid smoothing is used to minimize skewness and kinks within the grid. INGRID has many options for smoothing the grid. Experience with the smoothing options determined that the P.D. Thomas Forcing Function (Option Number: -3, in INGRID) worked the best. A small amount of smoothing over the entire grid gave the best results.

The grid coordinates are saved in a file by INGRID once the grid has been refined to satisfaction. This coordinate file is combined with a initial flow field file for input to the PARC code.

PARC Code

The input needed to execute the PARC code is a re-start file. The re-start file consists of code variables and the flow field file from the previous iteration session. The inputs for the PARC code can be generalized into five major groups:

1. Fluid properties.
2. Boundary conditions.
3. Convergence controls.
4. Output controls.
5. Grid dimensions.

The PARC inputs are too numerous to list here. See the PARC manual for descriptions of each input variable [9]. An example of a PARC re-start file for the turbulent calculations is shown in Figure A-2. The re-start file is in JCL (Job Control Language) format to communicate with the computer operating system at Marshall Space Flight Center

```
****** ****************************** TOP OF DATA **************
000001 //CFGC196A JOB (6EP506590341),'COLLINSBIN196.159%',
000002 //   MSGCLASS=X,CLASS=A,NOTIFY=CFGC196
000003 //   EXEC CRAY
000004 //SYSIN  DD *
000005  CRSUBMIT F(INPUT) HOLD NOTIFY(CFGC196) SUB(CSS2)
000006 //INPUT  DD *
000007 JOB,JN=CFGC196,MFL=1486160,T=89.
000008 ACCOUNT,AC=6EP506590341,US=CFGC196.
000009 FETCH,DN=SOURCE,TEXT='DSN=CFGC196.PDS.FORT(ORR2D2),DISP=SHR'.
000010 FETCH,DN=FT02,TEXT='DSN=CFGC196.AAA.DATA(SSOUT10),DISP=SHR'.
000011 CFT,I=SOURCE,L=0.
000012 LDR,L=0.
000013 DISPOSE,DN=FT04,DC=ST,WAIT,   ^
000014         TEXT='DSN=CFGC196.TURB1.DATA(SSOUT16),DISP=SHR'.
000015 /EOF
000016  &INPUTS
000017   NMAX=2, JMAX=210,      KMAX=120,     PREF=3000.0,
000018   TREFR=6600.0, GAMMA=1.200,   RE=3529392.00,  PR=.72,  PRT=.90,
000019   TSUTH=1550, INVISC(1)=1, INVISC(2)=1, LAMIN(1)=0, LAMIN(2)=1,
000020   IAXISY=1,       STOPL2=1.E-10, NP=2, NPSEG=1,
000021   NSPRT=10,    IFXPRT=1,      L2PLOT=0,     IFXPLT=0,
000022   DIS2=0.25,     DIS4=0.64,   DTCAP=0.40, PCQMAX=.40,
000023   IVARDT=2,
000024  &END
000025  &PRTSEG
000026   JKLPI(1,1,1)=1,210,1,JKLPI(1,2,1)=1,120,1,IPORD(1)=2,
000027  &END
000028  &BOUNDS
000029   NJSEG=2,
000030     JLINE(1)=1,
000031       JKLOW(1)=2,   JKHIGH(1)=119,      JTYPE(1)=0,
000032       JSIGN(1)=1,   PRESSJ(1)=.833333,  TEMPJ(1)=1,
000033     JLINE(2)=210,
000034       JKLOW(2)=2,   JKHIGH(2)=119,      JTYPE(2)=0,
000035       JSIGN(2)=-1,  PRESSJ(2)=.00001,  TEMPJ(2)=1,
000036   NKSEG=2,
000037     KLINE(1)=1,
000038       KJLOW(1)=1,   KJHIGH(1)=210,      KTYPE(1)=51,
000039       KSIGN(1)=1,
000040     KLINE(2)=120,
000041       KJLOW(2)=1,   KJHIGH(2)=210,      KTYPE(2)=60,
000042       KSIGN(2)=-1,
000043  &END
```

Figure A-2. Sample PARC Re-start File.

(MSFC). Information on the JCL format can be found in [22]. The re-start files for all flow field calculations are similar. Their differences will be discussed in the following paragraphs.

The flow field from the previous iteration is represented by four nondimensional quantites calculated at every grid node and output to an end-file (SSOUT16 in Figure A-2) by the PARC code. The four quantities are: density, axial and radial momentum, and total energy per unit volume. These quantities, combined with the grid coordinates, are input as the re-start file (SSOUT10 in Figure A-2) during an iteration session. The file for the very first iteration session is created by combining the grid coordinate output file from the INGRID code with an arbitrary initial flow field file. For the arbitrary initial flow field, the nondimensional density was set to unity; the nondimensional momentum terms to zero; and the energy term to the following expression of gamma:

$$\frac{1}{\gamma(\gamma - 1)}$$

The fluid property inputs for the re-start file were determined by arbitrarily assuming the nozzle fluid was steam. The choice of steam was based on the fact that the

products of combustion for the real rocket nozzle are mainly steam. Below is a list of the fluid properties input to the restart file of the PARC code:

Temperature = 6600 ^{o}R

Pressure = 3000 psia

Gamma = 1.2

Prandtl Number = .72 (=.90 for turbulent calculations)

Reynolds Number = 3,529,392 per foot

Sutherland Temperature = 1550 ^{o}R

Again,it should be stressed that the PARC code used for this study does not have real gas and chemical reaction capabilities. Therefore, the flow field properties and the performance levels for the nozzle are relative, not absolute.

The PARC code has options for manipulating the Navier-Stokes equations. These parameters are identified as INVISC and LAMIN in the re-start file of Figure A-2. INVISC (1) corresponds to the axial direction and INVISC(2) corresponds to the radial direction. Likewise for the LAMIN parameters. The values for INVISC and LAMIN were different for the inviscid, laminar, and turbulent calculations. INVISC and LAMIN values were set to zero for the inviscid calculations. These choices convert the

Navier-Stokes equations into the Euler form. For the laminar calculations both INVISC parameters were changed to one while both LAMIN parameters remained zero. This arrangement incorporates the viscous stress terms in both directions to the Navier-Stokes equations. INVISC values were set to one for the turbulent calculations while LAMIN(1) was zero and LAMIN(2) was one. This arrangement incorporates the Baldwin-Lomax algebraic turbulence model into the calculations. The turbulence model is applied in the radial direction only, but the viscous terms are retained in both the radial and stream-wise directions [8,11,15,16].

The boundary conditions for all calculations are represented in the re-start file as the JTYPE and KTYPE parameters. Each of the four exterior boundaries has a corresponding JTYPE or KTYPE parameter. All boundaries are constant index lines. For example, the nozzle wall is the K=120 constant index line and is identified as KTYPE(2)=60 for the viscous calculations. The value of 60 represents the boundary condition of a no-slip, adiabatic wall. The wall boundary condition for the inviscid calculations was slip, adiabatic wall (KTYPE(2)=50)). The in-flow and out-flow boundary conditions for all calculations was the free boundary condition (JTYPE(1), JTYPE(2)=0). The centerline of the nozzle was always the

axis of symmetry boundary condition (KTYPE(1)=51). The boundary conditions were kept constant during the iteration process for all calculations.

The convergence process for the inviscid, laminar, and turbulent flow field calculations were different. First, the generalities of the convergence process will be discussed before pointing out the procedural differences between flow field calculations.

The convergence process for all calculations was started after generating the computational grid with the INGRID code and determining the inputs for the initial re-start file. The convergence process is subdivided into smaller segments called iteration sessions. Sessions were typically 500 to 2000 iterations in duration. The iteration sessions began by inputting the re-start file to the PARC code. The iteration sessions were completed by outputting an end-file for use as the restart file for the next iteration session.

The results of the iteration session were reviewed before beginning a new session. The results consisted of the convergence history and the flow field properties calculated in engineering units. The PARC code outputs these values to an interactive output file (IOF) that can be viewed on the terminal screen after each iteration

session. The IOF file provides the information needed to decide if the convergence process should continue. Figure A-3 shows examples of the solution convergence information contained in the IOF file.

The convergence history is a group of variables (L2,DT,MAX PERCENT VARIATION, and the FLUX terms) which give information on the convergence of the solution. This information can be used to modify the convergence controls (DTCAP,IVARDT,PCQMAX, etc.) in the re-start file to enhance convergence during the next iteration session.

The variable L2 is synonymous with residual or error. L2 is the norm of the right-hand-side of the continuity equation after it has been reduced to its approximate factorization form [1,4]. The objective of the convergence process is to make the L2 error term as small as possible. Ideally, L2 should approach machine zero (approximately 10E-13 on the CRAY) with increasing iteration number. An L2 level of 10E-10 was chosen to signify convergence for all flow field calculations.

L2 was not the only variable used to monitor convergence. The FLUX terms were also used. Similar to L2, convergence was indicated by the FLUX terms when their magnitude approached 10E-10. Also, one can't underemphasize the importance of viewing the plots of flow field data after every iteration session. Comparison of

COUNT	DT	L2 RESIDUAL	MASS FLUX	MOMENTUM FLUXES X	MOMENTUM FLUXES Y	ENERGY FLUX	MAX PERCENT VARIATION	MAX LOCATION J	MAX LOCATION K
9010	0.4000E+00	0.5783E-03	-0.5506E-05	0.3429E-03	0.7666E-04	0.1441E-03	0.2969E+00	209	94
9020	0.4000E+00	0.5777E-03	-0.2330E-05	0.3574E-03	0.9594E-04	0.1511E-03	0.2662E+00	121	77
9030	0.4000E+00	0.5661E-03	0.2562E-05	0.3764E-03	0.1431E-03	0.1611E-03	0.3200E+00	209	88
9040	0.4000E+00	0.5570E-03	0.3616E-05	0.3894E-03	0.1728E-03	0.1673E-03	0.2898E+00	209	87
9050	0.4000E+00	0.5614E-03	0.4324E-05	0.4020E-03	0.2022E-03	0.1729E-03	0.2608E+00	206	76
9060	0.4000E+00	0.5408E-03	0.1296E-04	0.4285E-03	0.2406E-03	0.1864E-03	0.2204E+00	208	79
9070	0.4000E+00	0.5368E-03	0.1973E-04	0.4514E-03	0.2863E-03	0.1973E-03	0.1881E+00	124	77
9080	0.4000E+00	0.5222E-03	0.1868E-04	0.4614E-03	0.3195E-03	0.2009E-03	0.1847E+00	209	96
9090	0.4000E+00	0.5161E-03	0.2025E-04	0.4762E-03	0.3381E-03	0.2083E-03	0.2108E+00	126	77
9100	0.4000E+00	0.5219E-03	0.2796E-04	0.5030E-03	0.3291E-03	0.2224E-03	0.2467E+00	126	78
9110	0.4000E+00	0.5223E-03	0.3656E-04	0.5312E-03	0.3360E-03	0.2374E-03	0.3028E+00	128	77
9120	0.4000E+00	0.5239E-03	0.4822E-04	0.5647E-03	0.3433E-03	0.2548E-03	0.3360E+00	129	77
9130	0.3325E+00	0.5371E-03	0.5561E-04	0.5881E-03	0.3513E-03	0.2663E-03	0.4000E+00	130	77
9140	0.3760E+00	0.5556E-03	0.5995E-04	0.6054E-03	0.3808E-03	0.2743E-03	0.4000E+00	131	77
9150	0.4000E+00	0.5195E-03	0.6647E-04	0.6273E-03	0.4262E-03	0.2845E-03	0.3747E+00	132	77
9160	0.4000E+00	0.5232E-03	0.6871E-04	0.6410E-03	0.4827E-03	0.2903E-03	0.3872E+00	133	77
9170	0.3871E+00	0.5391E-03	0.6318E-04	0.6404E-03	0.5244E-03	0.2892E-03	0.4000E+00	134	77
9180	0.3254E+00	0.5620E-03	0.5334E-04	0.6309E-03	0.5441E-03	0.2837E-03	0.4000E+00	135	77
9190	0.3143E+00	0.5674E-03	0.4200E-04	0.6181E-03	0.5519E-03	0.2764E-03	0.4000E+00	136	77

Figure A-3. Sample of PARC Interactive Output File Statistics.

the flow field data with existing data and theoretical calculations helped to understand and progress the solution.

Although all the convergence controls were experimented with at one time or another during this research, it was discovered that DTCAP was the only control variable that effectively enhanced convergence for this application of the PARC code. As a matter of fact, DTCAP was the only convergence control that was varied for all the calculations presented here. DTCAP is the time-step parameter and has a direct effect on the convergence rate. A DTCAP value of 5.0 was used for all initial re-start files. Once the flow field approached its steady-state solution the value of DTCAP was lowered in successive iteration sessions until the solution had converged.

This concludes the generalized comments about the convergence process. The different calculation cases will now be summarized and the uniqueness of each case will be pointed out.

The inviscid flow field calculations were obviously the easiest solutions to converge. It took roughly 3000 iterations with an initial DTCAP value set at 5.0 to approach the steady-state solution. From the IOF files were plotted Mach numbers along the wall and centerline to indicate when the approximate steady-state flow field was

reached. Other indicators that the flow field was near convergence were the constant DT values over many iterations and the small levels (approximately 10E-5) of the FLUX terms. When the solution was nearly converged the value of DTCAP was lowered from 5.0 in unit increments during the impending iteration sessions. L2 steadily decreased with iteration count and FLUX and L2 levels of 10E-10 were achieved after roughly 5000 iterations. Central processing unit (CPU) time for the inviscid solution was thirty minutes on the CRAY.

The convergence procedures varied for the four laminar flow field calculation cases. Only two of the four cases were able to converge. The other two cases exhibited stalled convergence, which was denoted by an oscillating L2 value with iteration count. In other words, the L2 value didn't steadily decrease with iteration count.

The Case 2 and Case 4 calculations exhibited stalled convergence with L2 oscillating around the 10E-5 level. Changing DTCAP and the other convergence controls did not lower L2. After the L2 level started to oscillate, lowering DTCAP did not appear to progress the solution. Thus, it was decided to iterate for only 2000 iterations after the L2 level started to oscillate. Comparison of the results for the core of the flow field to the inviscid core results show that this portion of the laminar flow

field had converged. Only the flow within the boundary layer was not converged.

The Case 3 laminar calculations proceeded similarly to the inviscid solutions. There were no signs of stalled convergence. After 5000 iterations it appeared that the core of the flow field had approached the steady state solution. Lowering DTCAP in continuing iteration sessions reduced L2 and the FLUX terms steadily until they reached the convergence level of 10E-10.

An existing enhanced artificial dissipation model (EADM) was input to the PARC code and applied to the Case 2 grid. The purpose of the EADM was to reduce the artificial dissipation within the numerics of the PARC code as the solution approached the nozzle wall. This should allow the viscosity of the fluid to predominate over the artificial dissipation within the boundary layer of the flow. Hopefully, the EADM will enhance convergence and result in boundary layer characteristics which match actual boundary layers.

The L2 was reduced for the Case 2 with EADM to 10E-10, the desired level of convergence. The convergence process was similar to the Case 3 laminar solution and the inviscid solutions.

The number of iterations for the converged laminar solutions (Case 3 and Case 2 with EADM) was roughly 8000

iterations. The corresponding CRAY CPU time was about one and a half hours.

The convergence procedures for the turbulent calculations were also unique. The convergence process was started with the Navier-Stokes equations set for a laminar solution (INVISC(1) and INVISC(2)=1, LAMIN(1) and LAMIN(2)=0). After 3000 iterations the equation parameters were changed to turbulent (INVISC(1) and INVISC(2)=1, LAMIN(1)=0, and LAMIN(2)=1). The reason for using the laminar parameters was to establish the nozzle flow field within a minimal number of iterations. Using the turbulent parameters in the initial restart file may have stalled the solution or caused the solution to stop altogether because of negative pressures or some other PARC code error.

The DTCAP level was held at 5.0 for the first 8000 iterations. After 8000 iterations it appeared that the core of the flow field was established. L2 was also oscillating at a level of 10E-4. The solution was continued with 1000-iteration sessions. DTCAP was lowered over the next 7000 iterations from 5.0 to a final level of 0.4.

Plots of flow field properties played an important role in the convergence process for the turbulent calculations. Boundary layer profiles of temperature, pressure,

and Mach number were inspected at three axial planes within the nozzle after every iteration session, beginning with iteration 6000. The information was obtained from the IOF file at the end of each iteration session. See Figure A-4 for an example of the flow field information contained in the IOF file.

The purpose of inspecting the profiles was to document the progress of the computations seperate from the convergence statistics. The usually helpful convergence statistics started oscillating too early in the iteration count to be useful indicators of solution convergence. The boundary layer profiles were still changing with every iteration session even though the convergence statistics were stalled.

The percent change in select boundary layer properties were calculated every iteration session. Eventually the percent change of the properties reached an acceptable level and started to oscillate in sign. The calculations were terminated after iteration 15,000 because the boundary layer profiles had not changed significantly during the previous iteration session. Typical comparisons of boundary layer properties between iteration 14,000 and 15,000 were within 3%. Table A-1 summarizes the percent changes for the turbulent solution iteration sessions at

VARIABLES AT J = 200

K	PRESSURE	TEMPERATURE	MACH NUMBER	TOTAL PRESS	U-COSINE	V-COSINE	X	Y
1	0.3074E+00	0.1429E+04	0.6017E+01	0.2990E+04	0.1000E+01	0.0000E+00	0.1212E+03	0.0000E+00
2	0.3074E+00	0.1429E+04	0.6017E+01	0.2990E+04	0.1000E+01	0.1677E-02	0.1212E+03	0.1911E+00
3	0.3074E+00	0.1429E+04	0.6017E+01	0.2990E+04	0.1000E+01	0.3370E-02	0.1212E+03	0.3824E+00
4	0.3074E+00	0.1429E+04	0.6017E+01	0.2990E+04	0.1000E+01	0.5060E-02	0.1212E+03	0.5739E+00
5	0.3073E+00	0.1429E+04	0.6017E+01	0.2989E+04	0.1000E+01	0.6748E-02	0.1212E+03	0.7653E+00
6	0.3073E+00	0.1429E+04	0.6017E+01	0.2989E+04	0.1000E+01	0.8434E-02	0.1212E+03	0.9565E+00
7	0.3073E+00	0.1429E+04	0.6017E+01	0.2989E+04	0.9999E+00	0.1012E-01	0.1212E+03	0.1147E+01
8	0.3073E+00	0.1429E+04	0.6017E+01	0.2989E+04	0.9999E+00	0.1179E-01	0.1212E+03	0.1338E+01
9	0.3072E+00	0.1429E+04	0.6017E+01	0.2988E+04	0.9999E+00	0.1347E-01	0.1212E+03	0.1527E+01
10	0.3072E+00	0.1429E+04	0.6017E+01	0.2988E+04	0.9999E+00	0.1514E-01	0.1212E+03	0.1716E+01
11	0.3071E+00	0.1429E+04	0.6017E+01	0.2988E+04	0.9999E+00	0.1680E-01	0.1212E+03	0.1904E+01
12	0.3071E+00	0.1429E+04	0.6017E+01	0.2987E+04	0.9998E+00	0.1845E-01	0.1212E+03	0.2091E+01
13	0.3070E+00	0.1429E+04	0.6017E+01	0.2987E+04	0.9998E+00	0.2009E-01	0.1212E+03	0.2276E+01
14	0.3070E+00	0.1429E+04	0.6017E+01	0.2987E+04	0.9998E+00	0.2171E-01	0.1212E+03	0.2460E+01
15	0.3069E+00	0.1428E+04	0.6017E+01	0.2986E+04	0.9997E+00	0.2333E-01	0.1212E+03	0.2642E+01
16	0.3068E+00	0.1428E+04	0.6017E+01	0.2986E+04	0.9997E+00	0.2493E-01	0.1212E+03	0.2823E+01
17	0.3067E+00	0.1428E+04	0.6017E+01	0.2986E+04	0.9996E+00	0.2652E-01	0.1212E+03	0.3001E+01

Figure A-4. Sample of PARC Interactive Output File Flow Properties.

Table A-1. Exit Plane Turbulent Boundary Layer Percent Changes

	ITERATION NUMBER				
	6000	8000	10,000	12,000	15,000
P_{36}	-6.9%	-0.2%	6.9	-0.1	0.0
T_{36}	-1.1%	0.0	1.1	0.0	1.2
M_{36}	0.8	0.0	-0.8	0.4	-0.8
P_{71}	0.4	-2.0	-1.3	-1.3	0.4
T_{71}	0.2	0.0	0.0	-0.8	0.0
M_{71}	-0.2	0.1	-0.2	0.7	0.0
P_{96}	0.8	-1.0	-1.7	0.1	0.2
T_{96}	4.1	1.6	3.2	2.3	-2.0
M_{96}	13.0	6.8	10.0	6.0	-0.5
P_{116}	1.1	-2.5	0.3	-0.8	0.5
T_{116}	5.0	2.0	8.0	5.3	-3.1
M_{116}	10.1	-16.0	3.8	-15.0	9.7%

P denotes pressure

T denotes temperature

M denotes Mach number

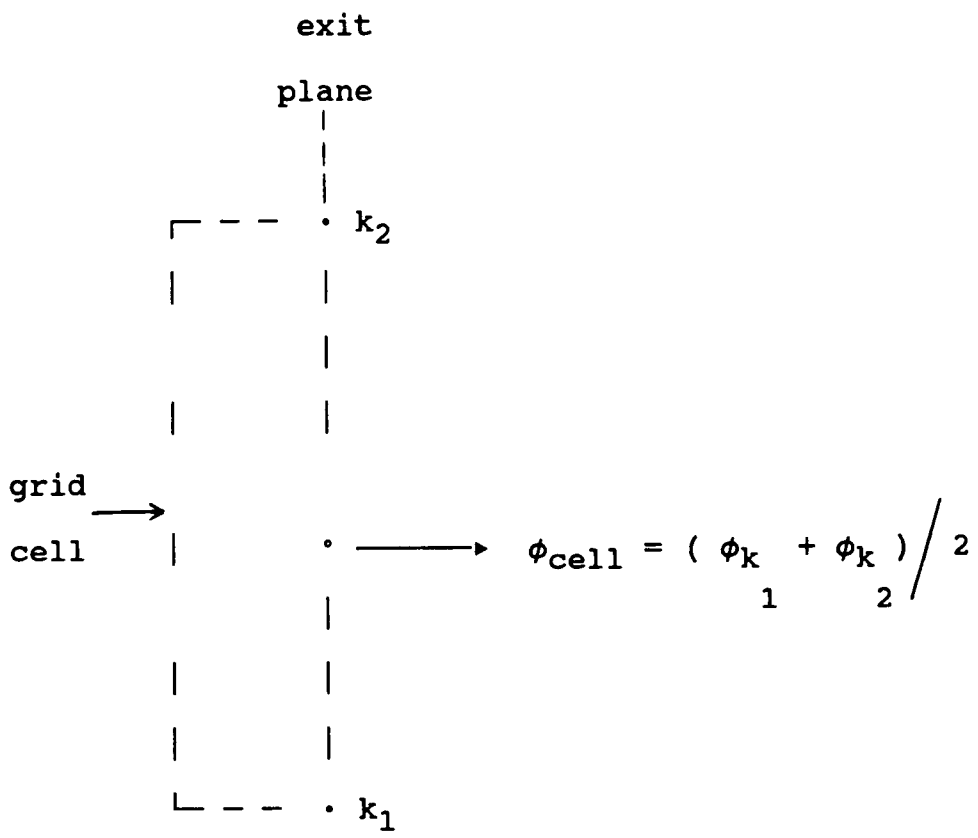
The subscript denotes the K-index for the grid at the exit plane. The exit plane represents a worst case summary.

Table A-1 reveals some interesting convergence trends. Solution convergence is denoted in the table by a small percent change number. The table shows that pressure was the first flow field property to converge. Mach number was the last. The properties near the embedded shock (K-index of 36) converge before the properties within the boundary layer, and they converge to a higher level or lower percent change. The temperatures within the boundary layer (K-index of 96 and 116) are increasing (denoted by a positive percent change) with iteration count until iteration 15,000. At 15,000 the temperature starts to decrease (negative percent change). Note that the pressures and Mach numbers within the boundary layer are oscillating in sign with iteration count. It was concluded that the change of sign in the percent parameter signified the culmination of the turbulent flow field solution.

APPENDIX B

NOZZLE PERFORMANCE SUBROUTINE EQUATIONS

The performance parameters were calculated by integrating the flow properties across the exit plane. The flow properties were averaged to give values which act at the center of the grid cells in the exit plane. See the following sketch:



The K-indices, k_1 and k_2, represent two nodes in the exit

plane. The flow properties at these nodes were averaged and acted at the center of the grid cell. The flow property is arbitrarily represented by the ϕ symbol. The property could be; pressure, temperature, etc..

Mass flow and thrust were calculated by summing (integrating) the contributions from each grid cell in the exit plane. Simpson's composite rule quadrature formula was applied to the mass flow and thrust summations to reduce the error of the calculations.

Below are the defining equations for the performance parameters:

$$\dot{m} = \sum_{i=1}^{n} (\rho_i A_i V_i)$$

$$T = \sum_{i=1}^{n} (\rho_i V^2_i A_i / g_c + (p_i - p_a) A_i)$$

$$Isp = \dot{m} / T$$

where,

$\dot{m}$ = total mass flow,

ρ = density,

A = cell area,

V = cell velocity,

T = total thrust,

g_c = gravitational constant,

p = static pressure,

p_a = ambient pressure

Isp = specific impulse,

n = number of grid cells in exit plane.

Figure B-1 contains the subroutine incorporated into the PARC code for performance parameter calculations.

```
003588        T=GAMMA*P(N)/R(N)
003589        AMACH=SQRT(VT2(N)/T)
003590        TT=T+0.5*GAMI*VT2(N)
003591        PT=P(N)*(TT/T)**GSGM
003592        PD=P(N)*GAMMA*PREF
003593        TD=T*TREFR
003594        PTD=PT*GAMMA*PREF
003595        UCOS=U(N)/VT
003596        VCOS=V(N)/VT
003597        WRITE(6,203)N,PD,TD,AMACH,PTD,UCOS,VCOS,XX(N),YY(N),VT
003598 C
003599 C
003600 C   WRITE THE VALUES TO ARRAYS FOR THE PERF SBRTNE. IF THE LOOP
003601 C   IS AT THE EXIT PLANE OR THE DESIRED J INDEX DESIGNATED BY VARIABLE
003602 C IA
003603        IF (IA .EQ. 200)THEN
003604             PERP(N)=PD
003605             PRAD(N)=YY(N)
003606             PERT(N)=TD
003607             PMACH(N)=AMACH
003608             PUCOS(N)=UCOS
003609        ENDIF
003610   203  FORMAT(1X,I5,9E12.4)
003611   305 CONTINUE
003612        IF(IA .EQ. 200)THEN
003613             CALL PERF(N,I2,PERP,PRAD,PERT,PMACH,PUCOS)
003614        ENDIF
003615        RETURN
003616        END
003617 C
003618 C
003619        SUBROUTINE PERF(N,I2,PERP,PRAD,PERT,PMACH,PUCOS)
003620        DIMENSION  PERP(120),PRAD(120),PERT(120),PMACH(120),PUCOS(120)
003621        DIMENSION RMASS(120), THRUST(120)
003622        PI=3.141593
003623 C
003624 C   THIS SUBROUTINE CALCULATES THE NOZZLE PERFORMANCE PARAMETERS
003625 C   AT A DESIGNATED PLANE.
003626 C   CHECK THE DIMENSION STATEMENTS TO ENSURE THAT THEY AGREE WITH
003627 C   WITH THE SIZE OF THE GRID.
003628 C   CHECK CONSTANTS SUCH AS G,R,MW,EXIT PRESSURE,ETC., TO MAKE SURE
003629 C   THEY ARE CORRECT.
003630 C   THE FOLLOWING IS A RTN TO ELIMINATE THE BL FROM THE PERF CALCS
003631 C CHOOSE THE VALUE FOR THE EDGE OF THE BL
```

Figure B-1. Computer Code of Performance Subroutine.

```
003640 C
003641       DO 100 J=2,I2
003642            AVT=(PERT(J)+PERT(J-1))/2
003643            AVP=(PERP(J)+PERP(J-1))/2
003644            AVM=(PMACH(J)+PMACH(J-1))/2
003645            AVCOS=(PUCOS(J)+PUCOS(J-1))/2
003646            RA=((PRAD(J)**2)*PI-(PRAD(J-1)**2)*PI)/144
003647            RDENS=AVP*144/(85.7603*AVT)
003648            VEL=AVCOS*AVM*57.542*SQRT(AVT)
003649            RMASS(J)=RA*RDENS*VEL
003650            THRUST(J)=(RDENS*VEL**2)*RA/32.174+(AVP-.03)*RA*144
003651   100 CONTINUE
003652 C
003653 C   NEXT IS THE SIMPSON'S RULE ROUTINE TO CALC. MASS AND THRUST SUM
003654 C
003655       XMO=RMASS(2)+RMASS(I2)
003656       XTO=THRUST(2)+THRUST(I2)
003657       XM1=0.0
003658       XM2=0.0
003659       XT1=0.0
003660       XT2=0.0
003661       L=1
003662       DO 200 K=1,I2-2
003663            M=2+K
003664            IF(L .EQ. 1)THEN
003665                XM1=XM1+RMASS(M)
003666                XT1=XT1+THRUST(M)
003667                L=L+1
003668            ELSE
003669                XM2=XM2+RMASS(M)
003670                XT2=XT2+THRUST(M)
003671                L=L-1
003672            ENDIF
003673   200 CONTINUE
003674       SUMASS=(XMO+2*XM2+4*XM1)/3
003675       SUMTHR=(XTO+2*XT2+4*XT1)/3
003676       RISP=SUMTHR/SUMASS
003677       WRITE(6,201)
003678       WRITE(6,202)
003679       WRITE(6,203) SUMASS, SUMTHR, RISP
003680   201 FORMAT(///,T20,'PERFORMANCE PARAMETERS')
003681   202 FORMAT(/,T10,'MASS FLOW', T30,'THRUST',T60,'ISP')
003682   203 FORMAT(/,T10,E10.4,T32,E10.4,T58,E10.4)
003683       RETURN
003684       END
003685 C
003686 C
003687       SUBROUTINE WREST
```

Figure B-1. (Continued)

APPENDIX C

IDEAL PERFORMANCE PARAMETER CALCULATIONS

Mass Flow

$$\dot{m} = \sqrt{\frac{g_c\, W}{R}} \cdot \left(\frac{\gamma + 1}{2}\right)^{\frac{-(\gamma + 1)}{2(\gamma - 1)}} \cdot \frac{P_t\, A^*}{\sqrt{T_t}}$$

$$= \sqrt{\frac{1.2(32.174)(18.02)}{1545.4}} \cdot \left(\frac{1.2 + 1}{2}\right)^{-5.5} \cdot \frac{(3000)(83.41)}{\sqrt{6600}}$$

$$= \underline{1223.5}\ lb_m/s$$

where,

γ = gamma, ratio of specific heats,

g_c = gravitational constant,

W = molecular weight,

R = universal gas constant,

P_t = nozzle chamber pressure,

T_t = nozzle chamber temperature,

A^* = nozzle throat area.

A nozzle discharge coefficient (C_d) can be applied to the mass flow equation to account for boundary layer and geometric effects at the nozzle throat. A nominal value of .9975 is suggested. Therefore, the mass flow would be:

$$\dot{m} = \dot{m} \cdot C_d = 1220.4\ lb_m/s.$$

Specific Impulse

$$Isp = \left(\frac{2\gamma R g_c T_t}{W(\gamma - 1)} \left[1 - (P_a/P_t)^{\frac{\gamma - 1}{\gamma}} \right] \right)^{\frac{1}{2}} \Big/ g_c$$

$$= \frac{\left(\frac{2(1.2)(1545.4)(32.174)(6600)}{.2(18.02)} (1 - (.00001)^{.1667}) \right)^{\frac{1}{2}}}{32.174}$$

$$= \underline{424.4 \text{ sec.}}$$

P_a = ambient pressure.

Thrust

$$F = \frac{\gamma M P_t A^*}{\sqrt{1 + \frac{\gamma - 1}{2} M^2}} \left(\frac{\gamma + 1}{2} \right)^{-\frac{\gamma + 1}{2(\gamma - 1)}} + [P_t (1 + \frac{\gamma - 1}{2} M^2)^{\frac{-\gamma}{\gamma - 1}} - P_a] \cdot \left(\frac{A^* (1 + \frac{\gamma - 1}{2} M^2)^{\frac{\gamma + 1}{2(\gamma - 1)}}}{M \left(\frac{\gamma + 1}{2} \right)^{\frac{\gamma + 1}{2(\gamma - 1)}}} \right)$$

$$= \frac{1.2(6)(3000)(83.4103)(1.1)^{-5.5}}{\sqrt{1 + .1(6)^2}} + \cdots\cdots\cdots\cdots\cdots$$

$$[3000(1 + .1(6)^2)^{-6} - .03] \cdot \frac{[83.4103(1 + .1(6)^2)^{5.5}]}{6(1.1)^{5.5}}$$

$$= \underline{507{,}740 \text{ lb}_f}$$

MOMENTUM INTEGRAL ANALYSIS FOR BOUNDARY LAYER GROWTH

The turbulent boundary layer growth along a section of the nozzle wall which resembled a flat plate was determined by evaluating the two-dimensional Karman momentum equation. The objective of the analysis was to compare the boundary layer growth indicated by the PARC turbulent flow field solution to an empirical calculation.

The general nonlinear Navier-Stokes momentum equation is:

$$\rho \frac{D\bar{V}}{Dt} = \rho g - \nabla p + \nabla \tau_{ij} \qquad [15].$$

The Navier-Stokes momentum reduces to:

$$\frac{d\theta}{dx} + (2 + H) \frac{\theta}{U_e} \cdot \frac{dU_e}{dx} = \frac{\tau_w}{\rho_e U^2_e} \qquad [15].$$

where

θ = momentum thickness,

H = momentum shape factor,

δ^* = displacement thickness,

U_e = velocity at outer edge of boundary layer,

ρ_e = density at outer edge of boundary layer,

dx = distance along flat plate,

τ_w = wall skin-friction stress.

The above equation can again be reduced to:

$$\frac{d\delta}{dx} + \left[1/f + \frac{(2-M)^2 + h}{M(1 + .5M^2)} \frac{dM}{dx} \right] \cdot \delta = \frac{\rho_w}{\rho_e} \frac{\tau_w}{fU^2_e \rho_w}$$

where

M = Mach number at boundary layer edge,

δ = boundary layer thickness,

$f = \theta/\delta$,

$g = \delta^*/\delta$,

$h = g/f$,

ρ_w = density at wall.

The above equation can be solved for δ by integration. The numerical integrations were calculated and tabulated in [26] for Mach numbers ranging from .1 to 10. The analysis in [26] has the following assumptions:

1. surface is a flat plate with or without favorable pressure gradient,
2. velocity distribution within boundary layer has power-law profile,
3. skin-friction relations were extrapolated from low-speed correlations,
4. ratio of specific heats was 1.4.

Putting the above equation into the form for use of the integral tables in [26] gives:

$$\delta_b = \underline{E}_b \cdot \frac{K(dx/dM)}{x^{1/7}} \cdot [\underline{A}_b]$$

The turbulent boundary layer growth was evaluated along the nozzle wall section defined by the points; x=100.6 inch along the centerline, and the exit plane. The above equation was evaluated twice; once for the x=100.6 inch point, and once for the exit plane point. The b-subscript denotes the location of these two points relative to the reference plane for both evaulations. The point of reference for both evaluations was the nozzle throat plane. This point of reference was assumed to be the start of the nozzle's boundary layer growth. The choice of the throat plane as the point of reference simplified the original equations in [26] by eliminating the terms with the a-subscript, which represented an arbitrary point of reference. One must refer to [26] for the tabular data. Below is the data extracted from the tables and other calculations needed for the boundary layer growth analysis:

Exit Plane

N = 7,

$\underline{A}$ = 54.56,

$\underline{B}$ = 100.52,

M = 4.29,

x = 9.242 ft,

K = .001066 $ft^{1/7}$,

dM = 4.29 - 4.203 = .087.

X = 100.6"

N = 7,

A = 53.8283,

B = 98.34173,

M = 4.203,

x = 1.7167,

dM = .087

The resulting boundary layer thicknesses were:

δ_{exit} = .835 ft,

$\delta_{100.6}$ = .787 ft.

Thus, the boundary layer growth along the wall section for the momentum integral method was:

δ_{calc} = .576 inch.

VITA

Joseph Lawrence Orr was born January 9, 1960 in Minneapolis, Minnesota. He attended the University of Minnesota and graduated in June, 1983 with a Bachelor of Science,Mechanical Engineering degree. He then worked for FluiDyne Engineering Corporation, Minneapolis, MN from July, 1984 to August, 1987 as a test engineer.

After gaining three years of experience as an engineer Joseph decided to seek an advanced engineering degree. He entered the University of Tennessee Space Institute in September, 1987 where he accepted a graduate research assistantship with the Center for Advanced Space Propulsion (CASP). The topic of his research was the application of the PARC computational fluid dynamics code to high-area-ratio nozzles, which was the source for this thesis material. In August, 1989 Joseph completed his studies at the Space Institute and received a Master of Science degree in Mechanical Engineering.

Joseph accepted a position as an engineer at General Electric, Aircraft Engines Division in September, 1989. He plans to continue working in the areas of nozzle testing analysis, and design.